Neuron

Article

Elevated calneuron-1, an accessory subunit of muscarinic receptors, induces frontotemporal dysconnectivity and schizophrenia-like deficits

Graphical abstract

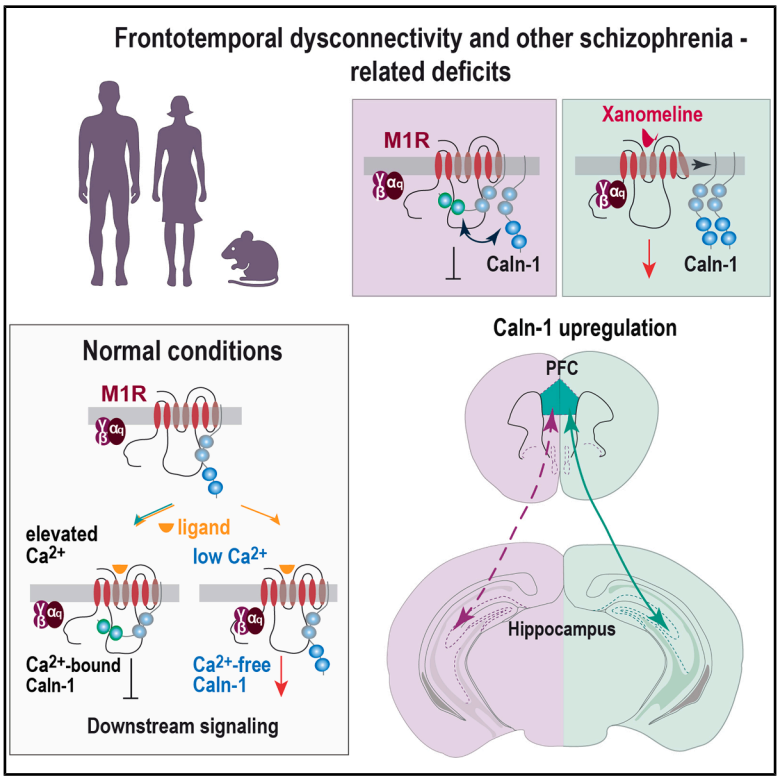

Highlights

- Calneuron-1 expression in the prefrontal cortex is elevated in schizophrenia
- Calneuron-1 overexpression elicits schizophrenia-related deficits
- Calneuron-1 is an accessory subunit of M1R that regulates muscarinic signaling
- The antipsychotic drug xanomeline disrupts the calneuron-1/M1R interaction

Authors

Anja M. Oelschlegel, Jastyn A. Pöpplau, Alexandre Ryzynski, ..., Ileana Hanganu-Opatz, Anna Karpova, Michael R. Kreutz

Correspondence

ileana.hanganu-opatz@zmnh.uni-hamburg.de (I.H..-O.), akarpova@lin-magdeburg.de (A.K.), michael.kreutz@lin-magdeburg.de (M.R.K.)

In brief

Oelschlegel et al. report that the schizophrenia-risk gene calneuron-1 is elevated in schizophrenia, elicits schizophrenia-like behavior, and impairs network communication in mice. Calneuron-1 is an accessory subunit of muscarinic M1R that inhibits G-protein coupling and shuts off M1R signaling in schizophrenia. The M1R agonist xanomeline interrupts calneuron-1/M1R interaction and rescues schizophrenia-related deficits.

Oelschlegel et al., 2026, Neuron *114*, 1–20
February 18, 2026
https://doi.org/10.1016/j.neuron.2025.10.038

CellPress

Neuron

CellPress
OPEN ACCESS

Article

Elevated calneuron-1, an accessory subunit of muscarinic receptors, induces frontotemporal dysconnectivity and schizophrenia-like deficits

Anja M. Oelschlegel,[1,15] Jastyn A. Pöpplau,[2,15] Alexandre Ryzynski,[1,15] Johannes Hradsky,[1,15] Pasham Parameshwar Reddy,[1] Gemma Navarro,[3] Irene Reyes-Resina,[1,3] PingAn Yuanxiang,[1] Liudmila Sosulina,[4,5] Hiroshi Kaneko,[4] Giriraj Sahu,[1,6] Anne Günther,[2] Maria Andres-Alonso,[1,7] Jeffrey Lopez-Rojas,[1,8] Ahmed A.A. Aly,[1] Pavol Bauer,[9] Sanja Mikulovic,[9,10] Zifeng Xia,[11] Marina Mikhaylova,[1,12] Stefan Remy,[4,10,13,14] Ileana Hanganu-Opatz,[2,16,*] Anna Karpova,[1,13,16,*] and Michael R. Kreutz[1,7,10,13,14,16,17,*]

[1]Research Group Neuroplasticity, Leibniz Institute for Neurobiology, Magdeburg, Germany
[2]Institute of Developmental Neurophysiology, Center for Molecular Neurobiology, Hamburg Center of Neuroscience (HCNS), University Medical Center Hamburg-Eppendorf, Hamburg, Germany
[3]Centro de Investigación Biomédica en Red Sobre Enfermedades Neurodegenerativas, Department of Biochemistry and Physiology, School of Pharmacy, University of Barcelona, Barcelona, Spain
[4]Department of Cellular Neuroscience, Leibniz Institute for Neurobiology, Magdeburg, Germany
[5]German Center for Neurodegenerative Diseases (DZNE), Bonn, Germany
[6]Molecular Biophysics Unit, Indian Institute of Science, Bengaluru, India
[7]Leibniz Group "Dendritic Organelles and Synaptic Function", Center for Molecular Neurobiology, ZMNH, University Medical Center Hamburg-Eppendorf, Hamburg, Germany
[8]Department of Psychology, University of Wisconsin-Milwaukee, Milwaukee, WI, USA
[9]Research Group Cognition & Emotion, Leibniz Institute for Neurobiology, Magdeburg, Germany
[10]German Center for Mental Health (DZPG), Magdeburg, Germany
[11]Department of Systems Physiology, Leibniz Institute for Neurobiology, Magdeburg, Germany
[12]Research Group Optobiology, Institute of Biology, Humboldt-Universität zu Berlin, Berlin, Germany
[13]Center for Behavioral Brain Sciences, Otto von Guericke University, Magdeburg, Germany
[14]German Center for Neurodegenerative Diseases (DZNE), Magdeburg, Germany
[15]These authors contributed equally
[16]These authors contributed equally
[17]Lead contact
*Correspondence: ileana.hanganu-opatz@zmnh.uni-hamburg.de (I.H.-O.), akarpova@lin-magdeburg.de (A.K.), michael.kreutz@lin-magdeburg.de (M.R.K.)
https://doi.org/10.1016/j.neuron.2025.10.038

SUMMARY

Calneuron-1 is a Ca^{2+} sensor that has been linked in several genome-wide association studies to schizophrenia (SCZ). We show that calneuron-1 expression is elevated in the dorsolateral prefrontal cortex of SCZ patients and that overexpression in the medial prefrontal cortex (mPFC) of mice elicits SCZ-related behavioral disabilities, disrupts rhythmogenesis within the mPFC, impairs functional connectivity between the hippocampus and the mPFC, and causes deficits in muscarinic synaptic plasticity. These neurophysiological signatures of SCZ are linked to the role of calneuron-1 as an accessory subunit of muscarinic M1 receptors (M1Rs). Calneuron-1 displaces $G\alpha q_{11}$ from the third intracellular loop of M1R at elevated $[Ca^{2+}]_i$, thereby disrupting downstream signaling. The M1R agonist xanomeline, shown to reduce positive and negative symptoms of SCZ and recently approved for clinical use, impedes this calneuron-1/M1R interaction, which leads to restoration of G-protein coupling, muscarinic synaptic plasticity, and network communication. Collectively, our data indicate a potential causative pathomechanism of SCZ.

INTRODUCTION

Schizophrenia (SCZ) is a complex, debilitating disorder that affects approximately 1% of the world population, with an onset in most cases in late adolescence/early adulthood. There is strong evidence for a genetic component of the disease,[1–5] in which both rare and common genetic variants contribute to risk. Among the strongest known factors is the 22q11.2 deletion, associated with mitochondrial dysfunction and synaptic deficits.[6–13] Disruption of *DISC1* impairs neurogenesis,[14–17] synaptic

Please cite this article in press as: Oelschlegel et al., Elevated calneuron-1, an accessory subunit of muscarinic receptors, induces frontotemporal dysconnectivity and schizophrenia-like deficits, Neuron (2025), https://doi.org/10.1016/j.neuron.2025.10.038

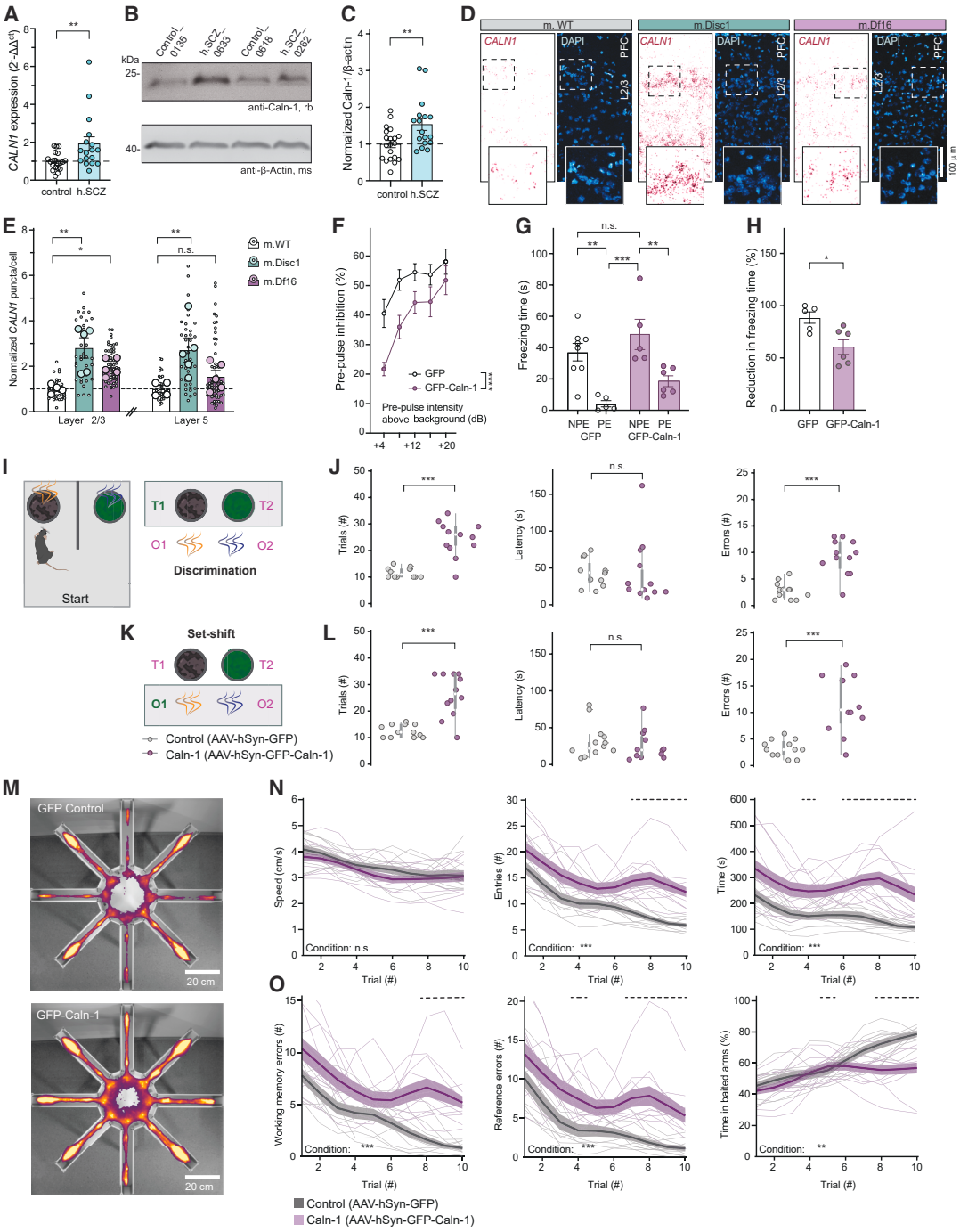

Figure 1. Elevated calneuron-1 levels accompany human SCZ and elicit SCZ-associated behavioral phenotypes in mice

(A–C) (A) *CALN1* transcript and (B and C) protein levels in postmortem PFC samples of SCZ patients (h.SCZ, $n = 17$) vs. controls ($n = 20$).

(D and E) *CALN1* mRNA expression in L2/3 and L5 of the PFC in two SCZ mouse models (m.Disc1 and m.Df16) vs. controls (wild type [WT]) (slices/mice: for L2/3 WT = 38/4, m.Disc1 = 41/5, m.Df16 = 62/5; for L5 WT = 38/4, m.Disc1 = 41/5, m.Df16 = 64/5; slices, small circles; mice, large circles).

(F) PPI in GFP ($n = 10$) vs. GFP-calneuron-1 ($n = 12$) mice; startling response following a lesser-intensity pre-tone; group analysis indicated as ****$p < 0.0001$.

(G and H) Latent inhibition: (G) absolute freezing time and (H) percentage reduction for non-pre-exposed (NPE; GFP = 8, GFP-calneuron-1 = 5) vs. pre-exposed (PE; GFP = 6, GFP-calneuron-1 = 6) mice.

(I–L) Discrimination and set-shift task. (I and K) Experimental protocol. (J and L) Trials to reach criterion, latency to dig, and errors during discrimination (J) and set-shifting (L) phase ($n = 12$ each).

(legend continued on next page)

plasticity,[18–21] dopamine signaling,[22–27] and mitochondrial function.[28,29] Variants in *NRG1/ErbB4* alter interneuron development and cortical inhibition,[30–42] while diminished *COMT* or the *COMT Val158Met* polymorphism are debated to modify prefrontal dopamine metabolism.[43–52] Further loci,[53] including *GRIN2A*,[54,55] *CACNA1C*,[56,57] *ZNF804A*,[58] and the *C4* gene within the major histocompatibility complex (MHC) region,[39,59] implicate glutamatergic dysfunction, calcium signaling, disrupted connectivity, and aberrant synaptic pruning. Despite their heterogeneity, these risk variants converge on shared pathophysiological processes, including GABAergic interneuron dysfunction, dopaminergic imbalance, NMDA receptor hypofunction, excessive synaptic pruning, mitochondrial impairment, and disrupted neurodevelopment.

The prefrontal cortex (PFC) has been shown to be highly relevant for the pathology, especially for negative symptoms and cognitive impairment.[60,61] Increasing evidence points to a significant role of muscarinic signaling in SCZ, shown to be impaired in human patients as well as in mouse models of the disease.[60,62,63] Muscarinic M1 receptor (M1R) activation induces long-term depression (LTD) at hippocampal-prefrontal-cortical (HP-PFC) synapses,[64] and indirect evidence for deficits in this type of LTD suggests a link to cognitive deficits and negative symptoms of SCZ.[60,65] Stimulation of M1R signaling has been shown to be sufficient to reduce both negative symptoms and memory impairments in an SCZ mouse model.[60] Encouraging results have been reported for xanomeline, an M1R/M4R agonist,[66] and the drug was most recently approved by the FDA for the treatment of SCZ in adults. Negative and cognitive symptoms of SCZ respond less to previously existing drugs, but xanomeline provides a new option for the management of SCZ, as it has been shown to improve both positive and negative symptoms. Currently, however, it is still unclear how muscarinic receptors contribute to the molecular pathology of SCZ.

Calneuron-1 is an EF-hand Ca^{2+}-sensor protein of the neuronal calcium-binding protein family.[67–70] In contrast to other calmodulin (CaM)-like Ca^{2+} sensors, it is a type II tail-anchored transmembrane protein that, after posttranslational insertion into the endoplasmic reticulum (ER), traffics through the secretory pathway.[71,72] Several genome-wide association studies (GWASs) propose that the human *CALN1* gene is a candidate SCZ risk gene.[4,73–81] In addition, there is evidence of upregulation of expression by Psychiatric Genomics Consortium (PGC3)-SCZ GWAS loci,[82] and a meta-analysis predicted that *CALN1* mRNA level might be upregulated in the dorsolateral PFC (dlPFC) of patients diagnosed with SCZ.[83] Accordingly, *CALN1* upregulation was indeed found in transcriptomic analyses of the human dlPFC in SCZ.[84,85]

At present, however, it is unclear how calneuron-1 expression and function can be related to psychotic behavior. Along these lines, despite the large number of genetic variants associated with SCZ, few causal variants are fully understood with regard to their respective pathomechanisms. Deciphering causal molecular pathomechanisms is crucial for applying these findings to prevention and treatment. Here, we provide evidence for a causal molecular pathomechanism of SCZ by demonstrating that calneuron-1 tightly interacts with M1R, disrupts G-protein coupling, and that elevated expression in the medial PFC (mPFC) leads to suppression of M1R signaling and frontotemporal dysconnectivity.

RESULTS

Calneuron-1 levels are elevated in the dlPFC of SCZ patients

Based on evidence that calneuron-1 transcript levels might be upregulated in SCZ,[84,85] we asked whether calneuron-1 expression might be elevated in the dlPFC of human patients (Figures 1A–1C). We obtained shock-frozen tissue samples from patients diagnosed with chronic SCZ, along with age- and sex-matched controls. *CALN1* mRNA levels, as evidenced by qPCR, were significantly higher in SCZ patients compared with controls (Figure 1A). In addition, we observed elevated levels of calneuron-1 protein (Figures 1B and 1C). Controlling for an effect of "smoking status" and "sex" on mRNA and protein levels revealed no main effect of cofactors and only a mild interaction ($p = 0.0497$) for "group" and "smoking status" that did not remain significant after post-hoc analysis (Figure S1A). The effect of the duration of the illness was also assessed in the SCZ group (Figure S1B) but did not show a significant correlation for either mRNA or protein levels. Also, M1R protein levels remained unchanged (Figure S1C). These findings suggest that elevated calneuron-1 expression is one signature of the molecular pathology of SCZ.

Calneuron-1 levels are elevated in mouse models of SCZ, and calneuron-1 overexpression in the mPFC elicits psychotic behavior

We determined *CALN1* mRNA levels in two mouse models mirroring the cognitive disabilities and network abnormalities present in SCZ patients. Disc1 mice carry a mutation in the *DISC1* gene, which is involved in brain development and neuronal function and potentially contributes to the risk of SCZ and related mental illnesses.[86] Df16 mice model the 22q11.2 deletion syndrome, a strong genetic risk factor for SCZ.[87] Both mouse models exhibit prominent dysfunction in the mPFC network as well as cognitive disabilities,[88–92] and qPCR revealed a significant upregulation of *CALN1* mRNA expression in their mPFC (Figure S1D). Subsequent RNAscope experiments localized this increase mainly to layer 2/3 and to a lesser degree to layer 5 (Figures 1D and 1E).

To test whether elevated calneuron-1 protein levels in the mPFC of wild-type mice can cause behavioral phenotypes associated with SCZ. Calneuron-1 is expressed in excitatory and inhibitory neurons (https://portal.brain-map.org/). Using a viral construct expressing calneuron-1 under a neuronal synapsin

(M–O) Working memory in GFP and GFP-calneuron-1 mice ($n = 11$ each). (M) Heatmaps of time per location; (N) speed, arms visited, and trial time; and (O) working memory errors, reference errors, and relative time in baited arms. Black stripes indicate trial-level significance. Data presented as mean ± SEM (A, C, E–H, N, and O) or median (white circle) with 25th and 75th percentile (gray whiskers) (J and L). $^{*}p < 0.05$, $^{**}p < 0.01$, $^{***}p < 0.001$.
See also Figure S1 and Table S2.

Please cite this article in press as: Oelschlegel et al., Elevated calneuron-1, an accessory subunit of muscarinic receptors, induces frontotemporal dysconnectivity and schizophrenia-like deficits, Neuron (2025), https://doi.org/10.1016/j.neuron.2025.10.038

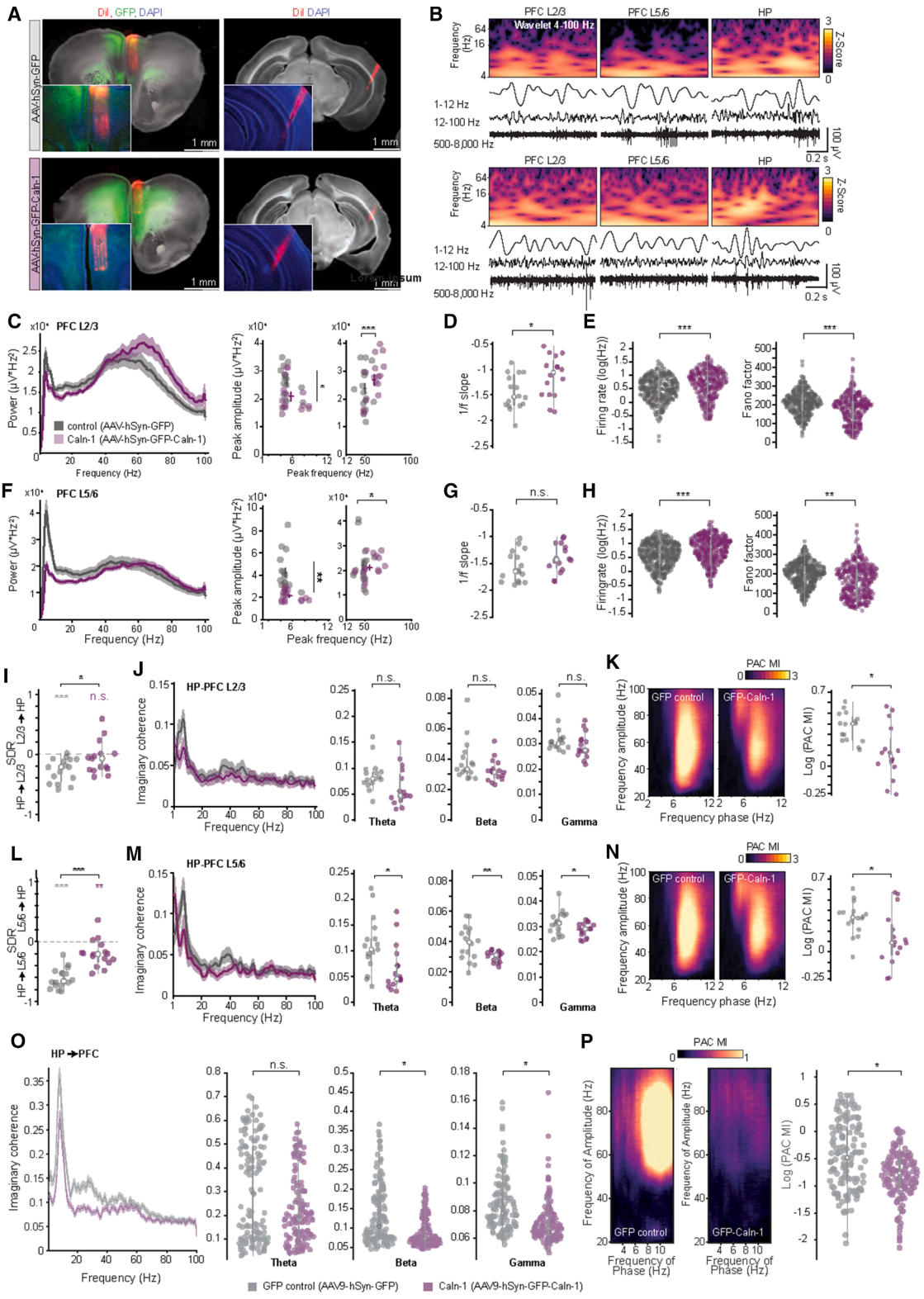

(legend on next page)

promoter in both cell types (Figures S1E and S1F), we infected a large number of neurons, particularly in layer 2/3 of the mPFC, as evidenced by GFP-fluorescence (Figure S1F). mRNA expression levels were higher but not vastly different from those in m-Disc1 mice (Figure S1G). Following 3 weeks of expression, we subjected adult mice to a battery of different tests. Behavior in an open-field arena was not altered (Figures S1H–S1J). Mice with elevated calneuron-1 levels in the mPFC displayed impairments in novelty exploration and recognition (Figures S1K and S1L). Novel object recognition in rodents is partially analogous to human declarative (episodic) memory, one of the cognitive domains, which is abnormal in SCZ.[93] Sensorimotor gating, measured by pre-pulse inhibition (PPI), is a fundamental form of information processing that is deficient in SCZ patients, and impairment in humans correlates with *CALN1* gene expression.[73] Similarly, PPI was clearly impaired in these mice (Figures 1F and S1M). Latent inhibition is another behavioral paradigm used to test for cognitive deficits in SCZ.[94] The disruption of latent inhibition is thought to result from an inability to ignore irrelevant stimuli, and we found corresponding deficits in mice following overexpression of calneuron-1 in the mPFC (Figures 1G and 1H).

Elevated calneuron-1 during development leads to long-lasting disruption of cognitive abilities

Deficits in cognitive flexibility and working memory are one of the first signs in individuals who are later diagnosed with SCZ, and these cognitive deficits might be caused by genetic alterations or early environmental impacts that interfere with normal brain development.[95–100] We infected neurons in the mPFC of wild-type mice at P5 (Figures S1N and S1O). In line with adult calneuron-1 overexpression, elevated levels of the protein during development caused no alterations in open-field behavior at juvenile or adult age (Figures S1P–S1R, S1W, and S1X). However, when assessing cognitive flexibility of juvenile mice in a four-choice discrimination and reversal task where the mice had to associate an odor with a reward, overexpression of calneuron-1 resulted in poorer performance (Figures S1S–S1V), indicating reduced cognitive flexibility. While during the initial discrimination phase no apparent differences were present (Figures 1S and 1T), the performance during reversal (i.e., switching the rewarded odor) was clearly lower, with more trials being required to reverse the previously learned rule and more errors occurring overall (Figures S1U and S1V). Next, we tested mice with developmental calneuron-1 overexpression in another cognitive flexibility task, a two-choice extradimensional set-shift task (Figures 1I–1L), where the mice have to associate a reward with the type of bedding or an odor, according to the relevant dimension. In contrast to juvenile age, adult mice already displayed disabilities during the initial discrimination phase (Figures 1I and 1J), which persisted during the set-shift phase (i.e., relevant dimension changes; Figures 1K and 1L), resulting in more trials and more errors occurring overall to reach the criterion. We also assessed whether working memory impairments are present at adulthood, using an 8-arm radial maze test. Mice overexpressing calneuron-1 showed markedly lower performance and made more working memory as well as reference errors. However, in line with the open-field tests, the speed of all mice was similar, confirming cognitive disabilities as being responsible for lower task performance (Figures 1M–1O). Notably, developmental calneuron-1 overexpression led to similar disabilities in novelty exploration and recognition (Figures S1Y and S1Z) as adult manipulation. Thus, elevated levels of calneuron-1 during development lead to a long-lasting disruption of cognitive abilities, which worsens with age. By considering that the used object and working memory tasks also involve other brain areas, such as the HP, the underlying network deficits are most likely not restricted to the mPFC.

Elevated levels of calneuron-1 during development disrupt prefrontal network activity and mPFC-HP communication

Abnormalities in synchronization and functional connectivity are thought to underlie behavioral phenotypes in SCZ.[101] To assess whether local elevation of calneuron-1 in the mPFC throughout development might impact neuronal and network activity, we performed electrophysiological recordings of local field potential (LFP) and single-unit activity (SUA) (Figures 2A and 2B) in all layers of the PFC and in the *stratum pyramidale* of the hippocampus at P30/31, 25/26 days post viral injection, in

Figure 2. Calneuron-1 overexpression during development and adulthood impairs frontal network activity and interregional network communication

(A) Coronal sections showing electrode positions in PFC (left, 32-channel, 4-shank) and HP (right, 16-channel, 1-shank) in GFP (top) and GFP-calneuron-1 (bottom) mice, and insets exhibit electrode positions in DAPI-stained sections at higher magnification.

(B) Exemplary LFP recordings and wavelet spectra of mPFC L2/3, L5/6, and HP during the resting phase.

(C) Left, LFP power spectra of mPFC L2/3; right, peak frequency (horizontal asterisks) as a function of peak amplitudes (vertical asterisks) for the 1–12 and 12–100 Hz bands, respectively.

(D and E) (D) 1/f slope of power-spectral densities and (E) firing rate and Fano factor of SUA recorded in mPFC L2/3.

(F–H) Same as (C)–(E) for LFP activity in mPFC L5/6.

(I–K) Assessment of simultaneously recorded activity in mPFC L2/3 and HP, (I) SDR, (J) imaginary coherence spectra and average imaginary coherence for 6–10 Hz theta, 12–30 Hz beta, and 30–100 Hz gamma bands, and (K) color-coded phase-amplitude coupling (PAC MI) matrix calculated between amplitude of 20–100 Hz activity in mPFC L2/3 and 1–12 Hz phase of HP activity, significance calculated for average of frequency-resolved matrix between theta phase and gamma amplitude.

(L–N) Same as (I)–(K) for mPFC L5/6 and HP.

(O and P) Same as (J), (K), (M), and (N) in mice overexpressing GFP or GFP-calneuron-1 only during adulthood.

For line plots, data are presented as mean ± SEM, and for others, as median (white circle) with 25th and 75th percentiles (gray whiskers). $^{*}p < 0.05$, $^{**}p < 0.01$, $^{***}p < 0.001$; (A–N) GFP-control, $n = 16$ recordings (8 mice, L2/3 354, L5/6 427, HP 281 single units); GFP-calneuron-1, $n = 16$ recordings (8 mice, L2/3 356, L5/6 418, HP 316 single units). (O and P) GFP-control, $n = 131$ areas (9 mice, 43 recordings); GFP-calneuron-1, $n = 133$ areas (8 mice, 39 recordings).

See also Figures S2 and S5 and Table S2.

non-anesthetized, head-fixed mice allowed to either move or rest in the Neurotar Mobile HomeCage system (Figure S1N). Following calneuron-1 overexpression, LFP recordings in L2/3 of the mPFC revealed lower band power for slower frequencies (1–12 Hz), while fast frequencies (12–100 Hz) tended to increase in power and were shifted toward higher frequency ranges (Figure 2C). Analysis of the aperiodic spectral features (i.e., the 1/f component of the log-log scale power spectrum) revealed a tilt slope toward less negative values (Figure 2D), indicating a shift in the excitation-inhibition ratio toward excitation.[102] Analysis of spiking activity revealed that elevated levels of calneuron-1 induced augmented firing of L2/3 neurons but less variable firing patterns (Figure 2E), indicating less complex spiking in these neurons. Similar disruptions of theta power, gamma frequency acceleration, and firing changes were present in layer 5/6 (Figures 2F–2H).

Abnormal activity in prefrontal layers following calneuron-1 overexpression might cause abnormal interlayer communication. We, therefore, assessed the directionality of signal transmission between layers by quantifying the spectral density ratio (SDR).[103] Control mice showed a drive from L2/3 to L5/6, which was prominently reduced in mice with elevated calneuron-1 (Figure S2A). Moreover, prefrontal synchrony was affected as mirrored by abnormal spike-phase and phase-amplitude coupling (Figures S2B and S2C). It has been shown that impaired theta phase coupling underlies frontotemporal (i.e., HP-PFC network) dysconnectivity in SCZ.[104] Therefore, we monitored HP activity as well as HP-mPFC communication. In line with the selective elevation of calneuron-1 in the mPFC, hippocampal network and neuronal activity, as well as theta-gamma-synchrony, were similar in both groups of mice (Figures S2D–S2G). Moreover, HP-specific sharp wave-ripples were not altered following calneuron-1 overexpression (Figures S2H and S2I). However, HP-mPFC communication was clearly impaired across all prefrontal layers as reflected by the lack of hippocampal drive to the mPFC in mice overexpressing calneuron-1 (Figures 2I and 2L). By contrast, the coupling synchrony between HP and mPFC in calneuron-1 mice, assessed by calculating the imaginary coherence, was mainly decreased in prefrontal layer 5/6 (Figures 2J and 2M). HP theta phase and mPFC gamma amplitude coupling were decreased in all prefrontal layers (Figures 2K and 2N). The abnormal HP-mPFC communication was also detected at the neuronal level, where fewer prefrontal units were significantly locked to the hippocampal theta rhythm in layer 5/6, and locking strength was reduced for both theta and gamma frequencies across all layers (Figures S2J and S2K). Collectively, these results show that developmental overexpression of calneuron-1 in the mPFC impairs interregional communication between the mPFC and the HP.

Overexpression of calneuron-1 in the mPFC of adult mice disrupts functional connectivity between the HP and the mPFC

We next assessed whether acute overexpression of calneuron-1 in the mPFC of post-adolescent mice induces similar functional dysconnectivity, indicating that elevated calneuron-1 alters signaling directly, irrespective of a possible role in development. To address this question, we injected wild-type mice at the age of 8 weeks to express either GFP or GFP-calneuron-1 in the mPFC. After testing these mice in PPI, electrodes were implanted bilaterally to assess the HP-mPFC circuitry with LFP recordings in a home cage environment. HP-mPFC communication was distinctly impaired in calneuron-1 overexpressing mice. Equivalent to overexpression during development, we found reduced theta (though not reaching significance), beta, and gamma band coupling synchrony between HP and mPFC by calculating the imaginary coherence (Figure 2O). Similarly, HP theta phase and mPFC gamma amplitude coupling were decreased (Figure 2P). Taken together, these data suggest that elevated calneuron-1 levels directly impair intra- and interregional network function irrespective of a possible role in development.

Elevated calneuron-1 levels disrupt mLTD in the mPFC

How could such changes be brought about? Several studies have established a link between M1R signaling and synaptic plasticity in the mPFC, and it has been shown that activation of M1R induces muscarinic LTD (mLTD) at HP-mPFC synapses.[60,64,105] Moreover, it is well documented that cholinergic neurotransmission is dysregulated in SCZ patients as well as in animal models of SCZ,[106–110] and cognitive impairments, as well as deficiencies in sensory gating, might be directly correlated with impairments of mLTD.[60] We induced mLTD in acute slices of the mPFC with bath perfusion of carbachol (Cch), as reported previously.[60] Overexpression of GFP-calneuron-1 induced a less pronounced decay of the field excitatory postsynaptic potential (fEPSP) slope, resulting in a significant attenuation of mLTD expression in the mPFC relative to controls (Figures 3A and 3B). Thus, elevating calneuron-1 protein levels is sufficient to disturb an SCZ-relevant form of muscarinic synaptic plasticity.

Calneuron-1 directly interacts with M1R

We found that virally expressed GFP-calneuron-1 co-localized with endogenous M1R in the mPFC (Figure 3C). Immunoprecipitation of endogenous calneuron-1 from rat brain lysates resulted in co-precipitation of M1R (Figure 3D) but not M3R (Figure S3A), suggesting that both proteins might be part of one complex. Heterologous co-immunoprecipitation corroborated an association of both HA- and GFP-tagged proteins in lysates of transfected HEK293T cells (Figure 3E). Proximity ligation assays (PLAs) confirmed the association of GFP-calneuron-1 with M1R in mPFC sections (Figures 3F, S3B, and S3C), as well as endogenous calneuron-1 with M1R in mature primary neurons prepared from the PFC (Figures 3G and 3H), isogenic i3Neurons derived from human i3-inhibitory postsynaptic currents (IPSCs) (Figures 3G and 3I), and mPFC sections (Figures 3G and 3J). Calneuron-1 differs in the EF-hand domain organization from other CaM-like calcium sensors, with a first functional Ca^{2+}-binding domain (EF-hand 1+2) and a non-functional second EF-hand domain (EF-hand 3+4/Figure S3D) incapable of Ca^{2+}-binding.[69] We observed weak but consistent binding of a GFP-calneuron-1 construct encompassing only the C terminus that includes the transmembrane domain (TMD) but lacks the two EF-hand domains (Figure 3K), whereas no association to the TMD of Syndecan-2, used as control, was found (Figure 3L).

Please cite this article in press as: Oelschlegel et al., Elevated calneuron-1, an accessory subunit of muscarinic receptors, induces frontotemporal dysconnectivity and schizophrenia-like deficits, Neuron (2025), https://doi.org/10.1016/j.neuron.2025.10.038

CellPress
OPEN ACCESS

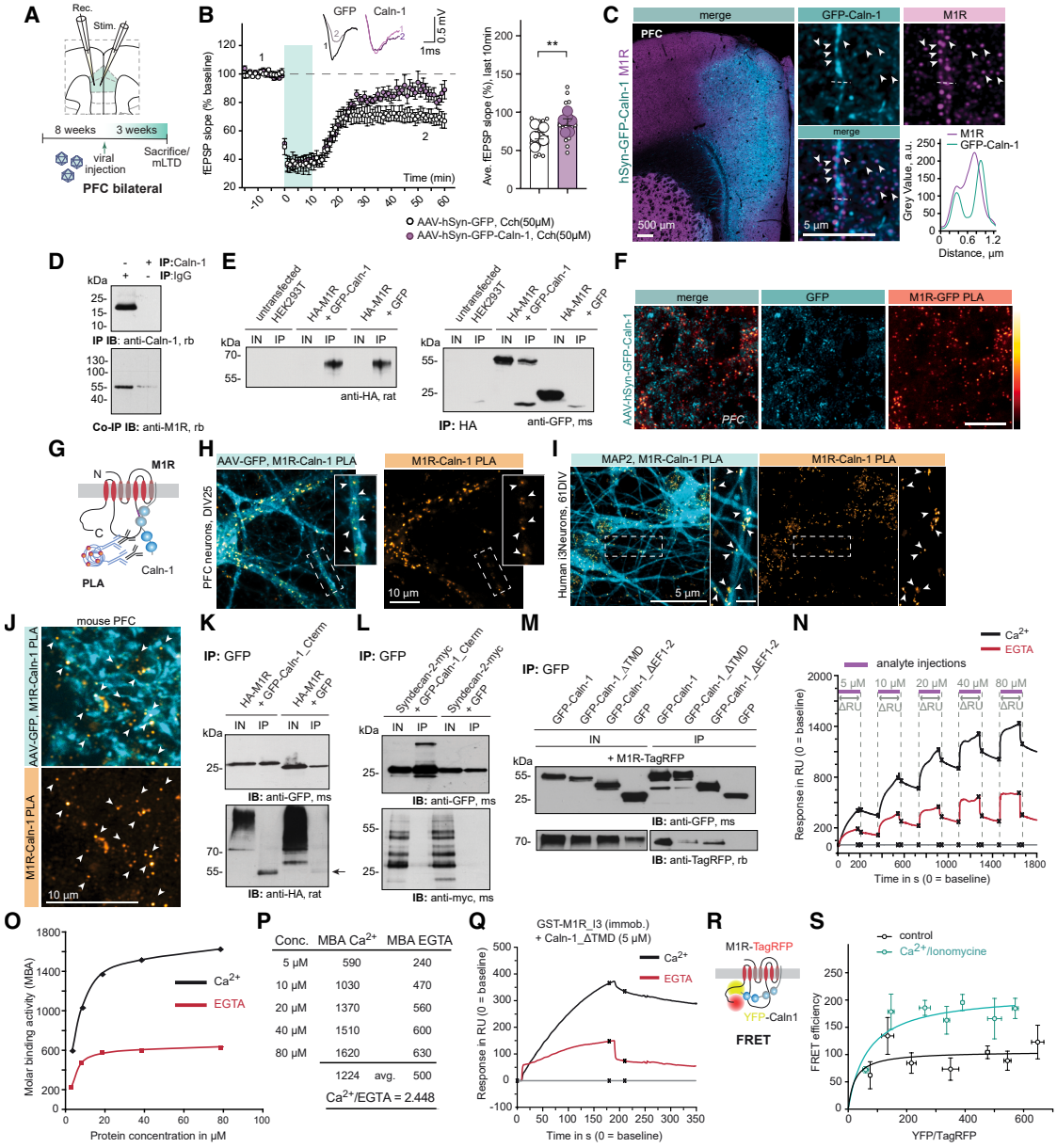

Figure 3. Elevated levels of calneuron-1 disrupt mLTD in the mPFC, and calneuron-1 directly interacts with M1R

(A and B) Cch-induced mLTD (50 µM Cch, 10 min; cyan box) in mPFC slices overexpressing GFP or GFP-calneuron-1; (A) timeline and electrode positioning, (B) representative fEPSPs with traces before (1) and after (2) induction, and average fEPSP slopes 50 min post-induction; GFP = 20 slices (6 mice), calneuron-1 = 22 slices (6 mice); slices/mice—small/large circles, $^{**}p < 0.01$.

(C) Confocal images of mPFC sections depicting GFP-calneuron-1 and endogenous M1R in L2/3 mPFC, and magnified images indicate colocalization (arrows) and position of line profile intensities (dashed lines).

(D and E) Co-immunoprecipitation of calneuron-1 with M1R in rat brain or transfected HEK293T lysates.

(F–J) *In situ* PLA depicting M1R association with (F) calneuron-1 after overexpression in mice or with endogenous calneuron-1 in (H) rat PFC primary neurons, (I) human i3Neurons, and (J) murine mPFC sections, and arrows in insets of higher magnification indicate PLA puncta.

(K–M) Co-immunoprecipitation of calneuron-1 transmembrane/C-terminal region and M1R.

(N–Q) SPR analysis of Ca^{2+}-dependent binding between calneuron-1_ΔTMD and the M1R I3 loop with (N) response and (O and P) MBA of Caln-1_ΔTMD at different concentrations in the presence of Ca^{2+} or EGTA; (Q) sensorgram of Caln-1_ΔTMD in the presence or absence of Ca^{2+}.

(R and S) FRET analysis in COS7 cells to validate Ca^{2+}-dependent calneuron-1-M1R interaction.

See also Figure S3 and Table S2.

Please cite this article in press as: Oelschlegel et al., Elevated calneuron-1, an accessory subunit of muscarinic receptors, induces frontotemporal dysconnectivity and schizophrenia-like deficits, Neuron (2025), https://doi.org/10.1016/j.neuron.2025.10.038

Clearly stronger interaction was evident in co-immunoprecipitation experiments when the TMD was fused to the second non-functional EF-hand domain (Figures 3M and S3D). Surface plasmon resonance analysis showed a direct interaction between the EF-hand-containing part of calneuron-1 (Caln-1_ΔTMD) and the I3 loop of M1R (Figures 3N and S3D). To calculate the molar binding activity (MBA) and the dissociation constant (K_D), we performed a single-cycle mode titration with the glutathione S-transferase (GST)-M1R-I3 loop coupled to the sensor chip and increasing amounts of calneuron-1_ΔTMD injected as the analyte (Figures 3N–3Q). Interestingly, the MBA of calneuron-1_ΔTMD in the Ca^{2+}-bound state exhibited a 2.4-fold increase compared with the Ca^{2+}-free state (Figures 3N–3Q) with an apparent K_D of 1.2 nM in the presence of Ca^{2+}. Even in the absence of Ca^{2+}, calneuron-1 displayed binding to the I3 loop, with a K_D of 39 nM. This suggests a tight association even at resting $[Ca^{2+}]_i$ levels. In direct comparison, equimolar amounts of other neuronal calcium sensors like Caldendrin (Figure S3E), CaM (Figure S3F), and NCS-1 (Figure S3G) showed no binding. Finally, to assess whether calneuron-1 associates with M1R in living cells, we performed Förster resonance energy transfer (FRET) assays in COS7 cells co-transfected with plasmids encoding for YFP-calneuron-1 and M1R-TagRFP. We indeed observed a stronger FRET signal with increasing levels of calneuron-1 (Figures 3R and 3S), and further augmentation was found following stimulation with the calcium ionophore ionomycin (Figure 3S).

To identify the binding interface within the intracellular loop 3 of M1R, we generated deletion mutants targeting two predicted CaM-binding motifs: a 1-8-14 motif and a partial IQ motif (Figures S3H and S3I). Both motifs are highly conserved across human, rat, and mouse M1Rs (Figure S3H) but are notably divergent in M3R and M5R (Figure S3J). GST pull-down assays demonstrated that simultaneous deletion of both motifs completely abolished ΔTMD-calneuron-1 binding, whereas deletion of either motif alone resulted in a partial reduction in binding affinity (Figures S3I and S3K). To further dissect the role of the 1-8-14 motif, we introduced point mutations substituting tyrosine 212 and leucine 225 with glutamate (Y212E/L225E), residues previously shown to disrupt CaM-binding (Figure S3I[111]). These substitutions markedly attenuated calneuron-1 binding in GST pull-down assays under both Ca^{2+}-containing and EGTA-buffered conditions (Figure S3K). Interestingly, the same mutations also significantly impaired Gαq binding, suggesting a shared or overlapping binding interface between calneuron-1 and Gαq (Figure S3L).

Sequence alignment of the 1-8-14 and IQ-like motifs in M1R with the corresponding regions in M4R revealed substantial divergence, indicating limited sequence conservation (Figure S3M). Consistent with this, PLA analysis showed that the calneuron-1/M4R interaction yielded significantly fewer PLA puncta relative to calneuron-1/M1R (Figures S3N and S3O).

Calneuron-1 binding to the I3-loop of M1R inhibits $G\alpha q_{11}$ coupling in a Ca^{2+}-dependent manner

M1R are coupled to $G\alpha q_{11}$ proteins to activate phospholipase C, leading to the production of inositol 1,4,5-triphosphate and diacylglycerol, which promote intracellular Ca^{2+} release and subsequent activation of PKC.[112,113] Agonist-independent pre-coupling of G-proteins to GPCRs is a common phenomenon,[114] and we indeed observed a decrease in the FRET signal between M1R and $G\alpha q_{11}$ with increasing levels of GFP-calneuron-1 expression (Figure 4A). Moreover, the effect of calneuron-1 overexpression was more pronounced after bath application of the Ca^{2+}-ionophore ionomycin (Figure 4A), indicating a Ca^{2+}-modulated displacement. Similar effects were observed when we performed the experiment with a calneuron-1 deletion mutant lacking the TMD (Figures 4B and S3D). Expectedly, we found that the first functional EF-hand domain is capable of displacing $G\alpha q_{11}$ from M1R after heterologous expression (Figure 4C). Conversely, overexpression of a deletion mutant lacking the EF-hand 1/2 domain (GFP-calneuron-1_ΔEF1/2) had no effect on the *in vitro* FRET signal between $G\alpha q_{11}$YFP and M1R-RFP (Figures 4D and S3D). $G\alpha q_{11}$ purified from SF9 cells did not directly interact with calneuron-1 (Figure S4A), whereas it bound to the I3 loop of M1R immobilized on a sensor chip (Figure S4B). In subsequent GST pull-down experiments, we corroborated interactions of both recombinant $G\alpha q_{11}$ and calneuron-1_ΔTMD to the GST-fused I3 loop (Figure 4E). Binding of calneuron-1_ΔTMD to the I3 loop was markedly enhanced in the presence of Ca^{2+} (Figure 4E). Most importantly, we observed displacement of $G\alpha q_{11}$ from the I3 loop when we added equimolar amounts of recombinant calneuron-1_ΔTMD to the buffer in the presence of Ca^{2+} (Figure 4E). Collectively, these data suggest that calneuron-1 masks the $G\alpha q_{11}$ binding site within the I3 loop of M1R in a Ca^{2+}-dependent manner.

Calneuron-1 regulates coupling of M1R to inhibitory synapses

We next wondered how the tight interaction between calneuron-1 and M1R might relate to the observed alterations in network activity following local overexpression in the mPFC, which suggests a shift in excitation-inhibition balance toward increased excitation (see Figure 2). Activation of M1R increases the frequency of spontaneous IPSCs (sIPSCs) and miniature IPSCs (mIPSCs) as well as the amplitude of sIPSCs via modulating $GABA_A$-receptor responses[115,116] and GABA release.[117] We therefore hypothesized that a loss of function of calneuron-1 should induce corresponding alterations in synaptic GABA release. To test this, we recorded mIPSCs in layer 2/3 of neurons in acute mPFC slices. We observed increased mIPSC amplitudes and frequencies in adult *CALN1* knockout mice (Figures 4F–4I). Thus, the data indicate that the loss of calneuron-1 causes increased $GABA_A$-dependent neurotransmission (Figures 4G–4I).

To investigate the role of calneuron-1 for synaptic inhibition by using medium spiny neurons (MSNs) that lack excitatory input, we recorded mIPSCs in rat striatal cultures in the presence of TTX in whole-cell patch-clamp configuration and found that shRNA knockdown of calneuron-1 increased mIPSCs amplitudes (Figures 4J, S4C, and S4D), consistent with our findings in acute slices. Pirenzepine, used at 1 μM, a concentration where it acts as an inverse M1R agonist,[118] blocked the effect of calneuron-1 protein knockdown (Figure 4J). Expectedly, bath application of Cch failed to increase mIPSC amplitudes in rat MSN overexpressing calneuron-1 (Figures 4K–4M and S4E).

Please cite this article in press as: Oelschlegel et al., Elevated calneuron-1, an accessory subunit of muscarinic receptors, induces frontotemporal dysconnectivity and schizophrenia-like deficits, Neuron (2025), https://doi.org/10.1016/j.neuron.2025.10.038

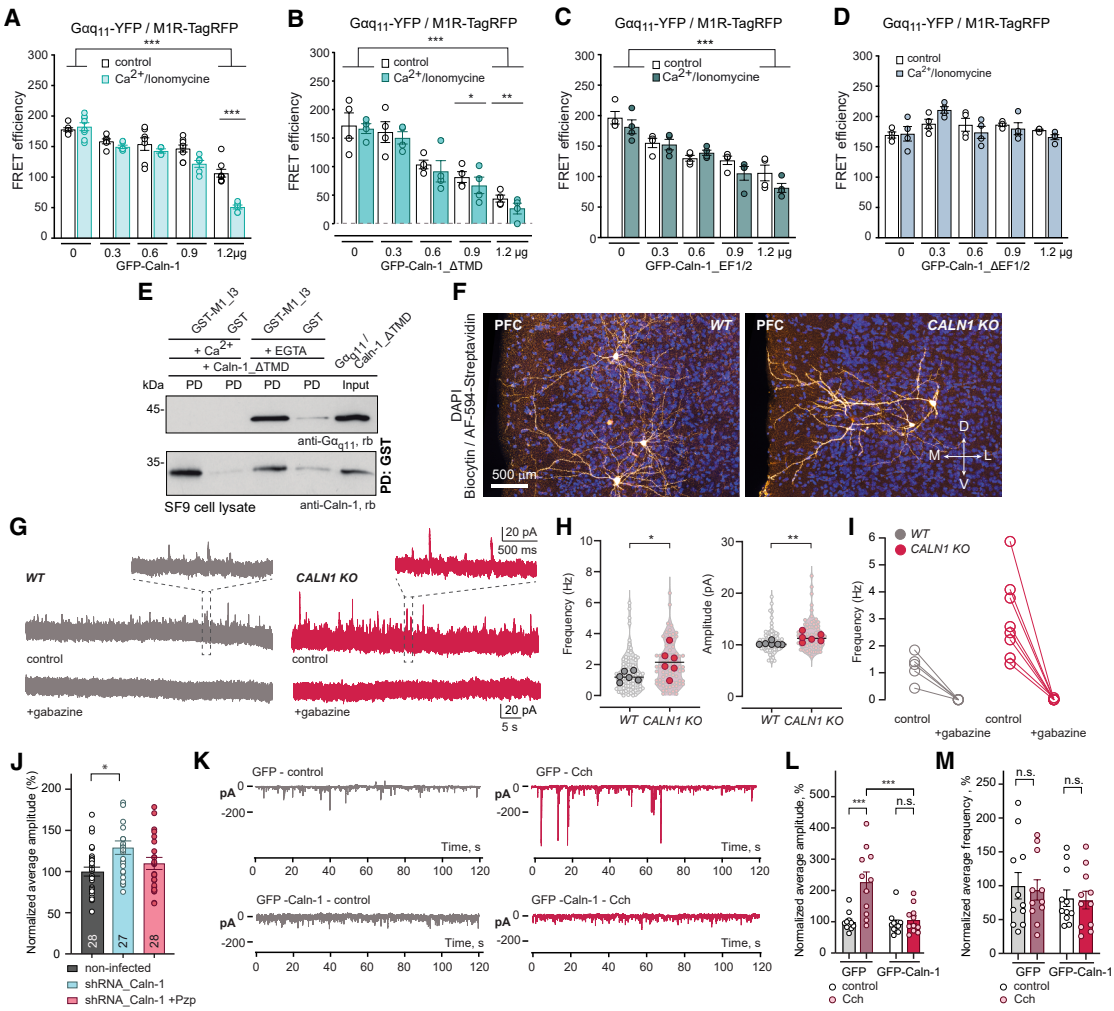

Figure 4. Calneuron-1 binding to the M1R I3-loop inhibits Gαq$_{11}$ recruitment in a Ca^{2+}-dependent manner and regulates coupling of M1R to inhibitory synapses

(A–D) FRET efficiency with or without Ca^{2+}/ionomycin at increasing expression levels of (A) GFP-calneuron-1, (B) calneuron-1_ΔTMD, (C) an EF-hand mutant (GFP-calneuron-1_EF1/2), or (D) calneuron-1 lacking the functional EF-hand domain.

(E) *In vitro* binding of calneuron-1_ΔTMD or Gαq$_{11}$ to the M1R I3-loop ±Ca^{2+}/EGTA.

(F) Confocal images of patched, biocytin-filled mPFC neurons in WT and *CALN1* knockout (KO) mice.

(G–I) mIPSC recordings from WT and *CALN1* KO mPFC neurons before and after gabazine (10 µM); (G) representative traces and (H) comparison of frequency or amplitude between genotypes; data presented as median of animals (large circles) with neuronal distributions (small circles); WT = 6 mice (80 cells/22 slices); KO = 6 mice (80 cells/23 slices); (I) all spontaneous events blocked by gabazine.

(J–M) mIPSCs from cultured striatal MSNs with calneuron-1 knockdown (shRNA_Caln-1) or overexpression (GFP-calneuron-1) compared with controls: (J) average amplitudes ±pirenzepine (Pzp, 1 µM); (K) representative traces recorded at −60 mV, and (L and M) normalized amplitude and frequency following Cch (10 µM). $^{*}p < 0.05$, $^{**}p < 0.01$, $^{***}p < 0.001$.

See also Figure S4.

Thus, in a cell culture system containing only MSN, we could isolate a functional interaction of calneuron-1/M1R with postsynaptic inhibitory responses that will likely cause changes in excitability in a neuronal network.

Xanomeline interrupts the interaction of calneuron-1 with M1R in excitatory neurons and restores G-protein coupling and synaptic plasticity in the mPFC

Next, we addressed whether the identified molecular mechanism represents a potential target for drug interventions in SCZ. Xanomeline is a muscarinic agonist acting on M1R and M4R that was shown to be effective in phase 3 trials in modulating psychotic and behavioral disturbances and correcting negative and cognitive symptoms.[66,119] It was recently approved by the FDA for the treatment of SCZ in adults (https://www.fda.gov/news-events/press-announcements/fda-approves-drug-new-mechanism-action-treatment-schizophrenia).

In experiments outlined above, utilizing PLA, we found evidence for a tight association of M1R with calneuron-1

Please cite this article in press as: Oelschlegel et al., Elevated calneuron-1, an accessory subunit of muscarinic receptors, induces frontotemporal dysconnectivity and schizophrenia-like deficits, Neuron (2025), https://doi.org/10.1016/j.neuron.2025.10.038

(Figures 3F–3J) but not with M4R (Figures S3M–S3O). Bath application of xanomeline significantly reduced PLA signal in i3Neurons (Figures 5A and 5B), indicating that the drug disrupts the interaction of the human proteins in a cellular context. Along these lines, xanomeline increased G-protein coupling in this experimental setting as evidenced by an increased PLA signal between M1R and $G\alpha q_{11}$ (Figures 5C and 5D), suggesting that muscarinic signaling can be restored by xanomeline. Complementary FRET assays showed that xanomeline indeed interrupts the interaction of M1R and calneuron-1 following heterologous expression (Figures 5E and 5F) and, most importantly, that xanomeline at a concentration of 5 μM restored G-protein coupling to M1R in the presence of calneuron-1 (Figure 5G). Moreover, we tested whether xanomeline might be effective to interrupt the interaction following overexpression of calneuron-1 in mice (Figures 5H and 5I). Like in human neurons, we observed reduced PLA signal in acute PFC slices treated with xanomeline, indicating reduced interaction between calneuron-1 and M1R (Figures 5H and 5I).

Xanomeline treatment also preserved SCZ-relevant muscarinic plasticity following calneuron-1 overexpression and rescued Cch-induced mLTD in acute slices of the mPFC (Figures 5J and 5K). Xanomeline administration had no effect on Cch-induced LTD (Figure S5A) and did alter expression of *CALN1* mRNA (Figures S5B and S5C).

The drug xanomeline-trospium (KarXT) combines xanomeline with the peripherally restricted muscarinic receptor antagonist trospium chloride[120,121] to ameliorate xanomeline-related adverse events associated with peripheral muscarinic receptors. As the FDA recently approved KarXT for the treatment of human SCZ patients (https://www.fda.gov/news-events/press-announcements/fda-approves-drug-new-mechanism-action-treatment-schizophrenia), we chose to combine xanomeline with trospium for an intervention *in vivo*. Mice, in which expression of either GFP or GFP-calneuron-1 was induced in the mPFC during adulthood (Figures 2O, 2P, 5L–5N, and S5G–S5J), received trospium once a day 2 h prior to a subcutaneous injection of xanomeline. Xanomeline treatment rescued calneuron-1 overexpression-induced behavioral deficits in PPI (Figure 5L). Similar to previous reports,[122,123] we found that xanomeline had a broad and complex modulatory effect on neurophysiological activity (Figures 5M, 5N, S5J, and S5K) and reduced locomotor activity (Figures S5H and S5I) in both GFP and GFP-calneuron-1 overexpressing mice. Analysis of the 1/f slope showed that vehicle-treated mice showed a shift toward excitation when compared with controls, whereas both xanomeline-treated groups showed a similar tilt (Figure 5M). The treatment normalized the excessive gamma power in the mPFC (Figure 5M), and most importantly, assessment of SDR revealed that xanomeline administration reinstated the directionality of signal transmission from the HP toward the mPFC, which was impaired in vehicle-treated calneuron-1 overexpressing mice (Figure 5N). Equivalent to the treatment-induced changes of the spectral mPFC LFP structure (Figures 5M and 5J), xanomeline also equalized mPFC-HP coupling synchrony between GFP and GFP-calneuron-1 overexpressing mice (Figure S5K). Hence, xanomeline treatment provided a functional rescue of network activity and HP-mPFC communication.

DISCUSSION

In this study, we show an increase of calneuron-1 levels in the dlPFC of SCZ patients. Given the heterogeneity in terms of medication, health status, status of smoking, and other factors (see Table S1), the upregulation of calneuron-1 expression appears to be a robust feature in SCZ patients. Similar results were obtained in two mouse models mirroring cognitive disabilities and network abnormalities present in SCZ patients. Accordingly, we found that local elevation of calneuron-1 protein levels during development and in adulthood alters the network activity in the mPFC, disrupts local prefrontal as well as HP-to-mPFC communication, impairs prefrontal mLTD in the mPFC, and elicits SCZ-related behavioral disabilities.

To unveil the underlying pathomechanism, we performed experiments demonstrating that calneuron-1 tightly associates with the I3 loop of M1R already at basal $[Ca^{2+}]_i$. The interaction involves Ca^{2+}-independent preassociation of the second nonfunctional EF-hand domain and subsequent Ca^{2+}-dependent binding of the first EF-hand domain, which interferes with $G\alpha q_{11}$ binding to the I3 loop and thereby inhibits M1R downstream signaling. We speculate that in a cellular context displacement of $G\alpha q_{11}$ interrupts M1R-induced modulation of $GABA_A$ receptors, which results in decreased amplitude of sIPSCs (mIPSCs/Figure 6). In line with these data, we propose that calneuron-1 might regulate an SCZ-relevant form of mLTD and contribute to the impairment of local network synchronization, resulting in dysfunctional interregional communication between HP and PFC. Accordingly, the muscarinic agonist xanomeline disrupts the interaction of M1R and calneuron-1, restores G-protein coupling and synaptic plasticity in the mPFC, reinstates HP-PFC directionality, and rescues behavioral deficits in PPI. KarXT is a muscarinic antipsychotic recently approved by the FDA for the treatment of SCZ. In combination with the peripheral nonselective anticholinergic trospium, xanomeline reduces psychotic symptoms, improves cognitive deficits, and has led to improvement in all symptoms of SCZ in phase 3 clinical trials.[66,119] Interruption of the calneuron-1/M1R interaction by xanomeline is highly suggestive for the involvement of calneuron-1 in SCZ and additionally points to a relevant molecular pathomechanism.

Calneuron-1 overexpression impairs HP-mPFC communication and PFC-dependent functions

To account for the developmental etiology of SCZ,[95–100] we investigated mice that experienced elevated levels of calneuron-1 during development and observed prominent dysfunctions in prefrontal activity as well as mPFC-HP communication that were detected already at juvenile age. This developmental local and long-range dysfunction was accompanied by impaired cognitive flexibility. Even at adult age, calneuron-1 mice exhibited poorer performance during the initial discrimination phase of cognitive flexibility tasks, suggesting that deficits persisted across development. The largely age-independent behavioral and functional phenotypes suggest that the calneuron-1 overexpression along the entire development and not at distinct time windows determines the degree of PFC-HP dysfunction and behavioral impairments.

Please cite this article in press as: Oelschlegel et al., Elevated calneuron-1, an accessory subunit of muscarinic receptors, induces frontotemporal dysconnectivity and schizophrenia-like deficits, Neuron (2025), https://doi.org/10.1016/j.neuron.2025.10.038

CellPress
OPEN ACCESS

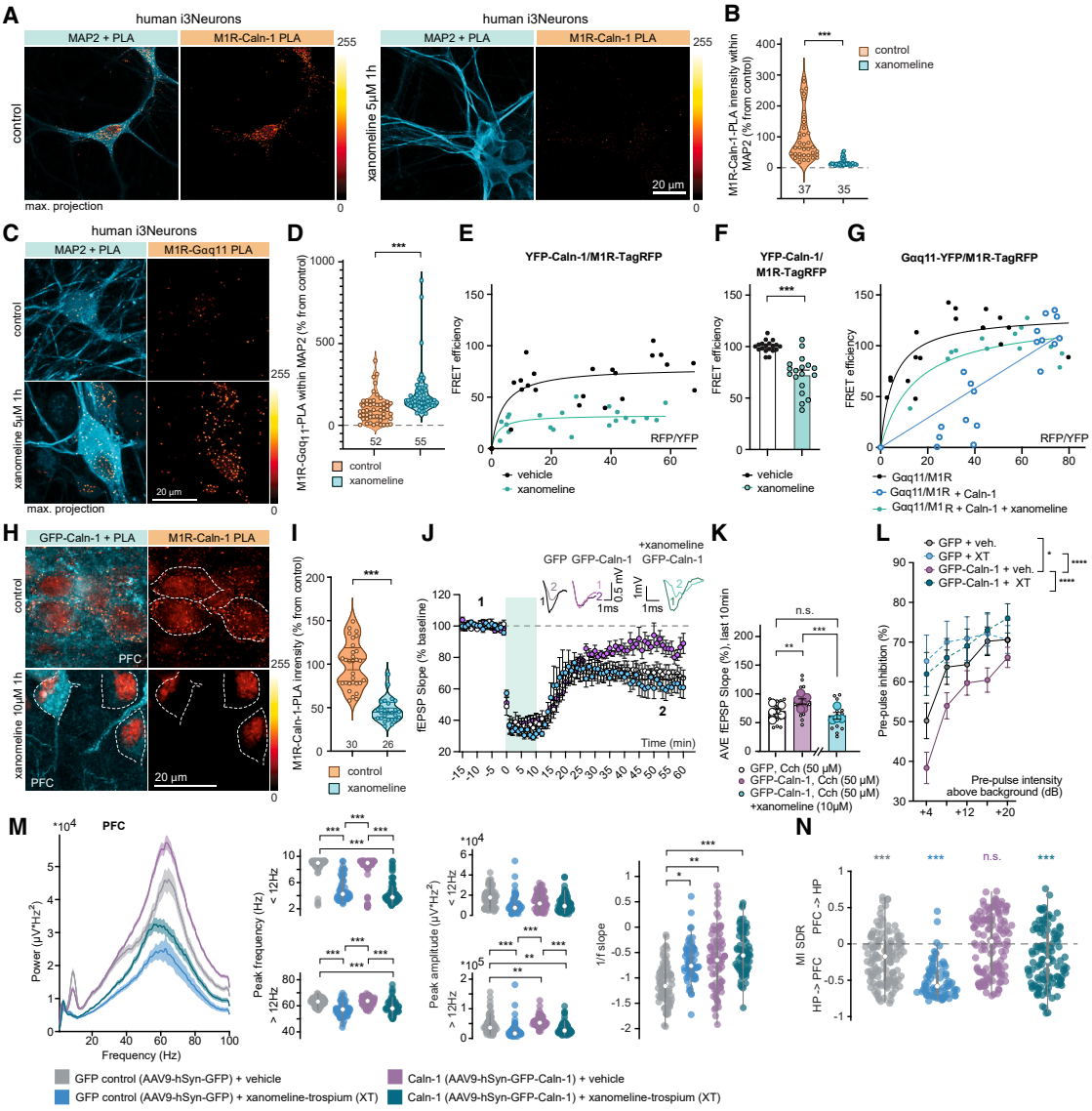

Figure 5. Xanomeline disrupts the calneuron-1-M1R interaction and restores G-protein coupling and synaptic plasticity in the mPFC

(A–D) PLA to determine association between calneuron-1/M1R or M1R/Gαq_{11} in i3Neurons (DIV61) ±xanomeline (5 µM, 1 h); PLA pixel intensity quantified within MAP2-defined regions of interest (ROIs); *n* = number of neurons, ***$p < 0.001$.

(E–G) FRET between YFP-calneuron-1 and M1R-TagRFP or Gαq_1-YFP and M1R-TagRFP following heterologous expression in HEK-293T cells ± calneuron-1-Rluc and/or xanomeline; data presented as mean ± SEM; ***$p < 0.001$.

(H and I) PLA in mouse PFC slices expressing GFP-calneuron-1 ±xanomeline (10 µM, 1 h); note nuclear background signal in control conditions due to the extensive number of labeled nucleotides.

(J and K) Cch-induced LTD in mPFC slices from GFP or GFP-calneuron-1 mice ±xanomeline (same as in Figure 3 for comparison); GFP-calneuron-1 + xanomeline, *n* = 18 slices (small circles) from 4 mice (big circles); **$p < 0.01$, ***$p < 0.001$.

(L–N) Xanomeline-trospium (XT) treatment *in vivo* in GFP and GFP-calneuron-1 mice. (L) PPI, GFP + veh (*n* = 10), GFP + XT (*n* = 9), calneuron-1 + veh (*n* = 15), calneuron-1 + XT (*n* = 9); group analysis indicated as *$p < 0.05$, ****$p < 0.0001$. (M) Left, mPFC power spectra of LFP activity; middle, peak frequencies and peak amplitude for 1–12 and 12–100 Hz frequency bands each. Right, 1/f slope of power-spectral densities. GFP-vehicle, *n* = 79 areas (10 mice, 46 recordings); GFP-XT, *n* = 64 areas (9 mice, 44 recordings); Cal-1-vehicle, *n* = 80 areas (10 mice, 46 recordings); and Cal-1-XT, *n* = 77 areas (9 mice, 44 recordings); *$p < 0.05$, **$p < 0.01$, ***$p < 0.001$. (N) SDR of simultaneously recorded activity in the PFC and HP. GFP-vehicle, *n* = 131 areas (9 mice, 43 recordings); GFP-XT, *n* = 79 areas (7 mice, 34 recordings); Cal-1-vehicle, *n* = 133 areas (8 mice, 39 recordings); and Cal-1-XT, *n* = 115 areas (8 mice, 39 recordings); *$p < 0.05$, **$p < 0.01$, ***$p < 0.001$. See also Figure S5 and Table S2.

Please cite this article in press as: Oelschlegel et al., Elevated calneuron-1, an accessory subunit of muscarinic receptors, induces frontotemporal dysconnectivity and schizophrenia-like deficits, Neuron (2025), https://doi.org/10.1016/j.neuron.2025.10.038

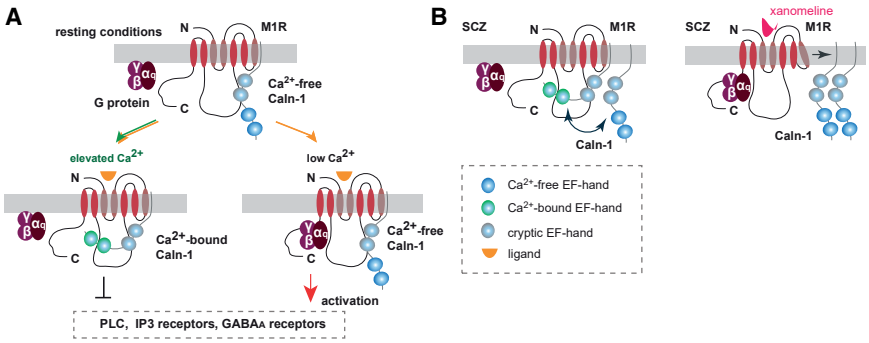

Figure 6. M1R regulation by calneuron-1 in the healthy and schizophrenic brain

(A) In the healthy brain, M1R and calneuron-1 pre-associate at resting $[Ca^{2+}]_i$ through the TMD and the second EF-hand domain of calneuron-1. As $[Ca^{2+}]_i$ rises, the first EF-hand domain displaces $G\alpha q_{11}$ from the M1R I3-loop.

(B) In the PFC of SCZ patients, enhanced calneuron-1-M1R association suppresses muscarinic signaling. Xanomeline dissociates this complex, restoring G-protein coupling.

The mPFC is one of the strongest interconnected brain regions, and most of its connectivity is reciprocal.[124] Consequently, an appropriate behavioral output depends on how received information is locally processed in the mPFC as well as on how downstream targets are instructed. Alterations in mPFC processing can therefore affect multiple neural circuits.[125] Consistent with this, we observed a broad range of behavioral impairments in adult mice overexpressing calneuron-1, including deficits in tasks that are not solely dependent on mPFC function. While the attentional set-shifting task primarily involves the mPFC, reversal learning depends more on the orbitofrontal cortex.[126,127] Both aspects of cognitive flexibility were impaired in calneuron-1 mice. Moreover, the working memory task revealed that not only short-term memory but also reference memory aspects are affected by the manipulation of the mPFC. This impairment of rather long-term memory storage points toward altered HP function. However, hippocampal activity appeared normal in both developmental and adult calneuron-1 overexpressing mice. By considering that the mPFC is crucial for retrieving information from long-term memory,[128,129] it is most likely that observed functional deficits in mPFC-HP communication account for the broad spectrum of behavioral disabilities during working memory but also object location tasks. Taken together, we propose that mPFC calneuron-1 overexpression leads to a comprehensive impairment of prefrontal circuitry and related behavioral functions irrespective of age.

Translational implications

Abnormal cognitive processing as a result of impaired prefrontal rhythmogenesis and connectivity are hallmark symptoms observed in both SCZ patients and animal models of the disease.[98,101,104,130,131] Here we found elevated calneuron-1 expression in the dlPFC of SCZ patients, as well as in the mPFC of two established mouse models—Df16 and Disc1—that are relevant to SCZ.[86,132] The dlPFC is a human-specific brain region, and its direct anatomical counterpart in mice remains highly debated. Mice differ from humans in connectivity patterns, parcellation, and layer structure of the PFC (e.g., lack of granular layer 4). Therefore, the direct comparison between species based on structural homology is challenging. More meaningful is a functional homology.[133,134] Prefrontal functions underlying the behavioral complexity and finesse characteristic of humans also exist, in a simpler form, in rodents, since they also require adaptive and flexible strategies in daily life. Moreover, the rodent mPFC shows a similar dorsal-ventral gradient in cognitive functioning as the primate PFC. Dorsal regions are more involved in decision-making and attention, whereas ventral regions support emotional and motivational processes.[101,124,133,135,136] Consistent with this functional homology, we showed that targeted overexpression of calneuron-1 in the mPFC of mice led to a broad range of functional and behavioral abnormalities that mirror those seen in SCZ patients and SCZ-related mouse models. Notably, locomotor and open-field behavior was not affected by prefrontal calneuron-1 overexpression, indicating that mainly adaptive and cognitive behaviors are disturbed. It is important to note that Df16 and Disc1 mouse models do not directly mimic a prefrontal dysfunction but rather mirror SCZ-related genetic abnormalities. *Disc1* orchestrates molecular cascades during brain development, such as cell proliferation and migration. The Disc1 mouse line carries a truncated version of the murine endogenous *Disc1* ortholog and has been shown to mirror many aspects of the identified SCZ-risk allele in humans.[86,91] The 22q11.2 microdeletion on human chromosome 22 represents a strong genetic risk factor for SCZ. The Df16 mouse model bears a hemizygous deletion syntenic to the 1.5 Mb critical region of 22q11.2 microdeletions in humans.[132] Both mouse models have been reported to have prefrontal network dysfunction and cognitive deficits at adult age.[88–92] Together, these findings suggest that elevated prefrontal calneuron-1 levels play a key role in driving SCZ-related symptoms, regardless of disease etiology, and may represent a convergent molecular pathomechanism.

Calneuron-1 is a calcium-sensing module of M1R that regulates G-protein coupling

This study also provides an in-depth dissection of the pathomechanism introduced above. We found that calneuron-1 and M1R tightly associate with very high nanomolar affinity already at resting $[Ca^{2+}]_i$. Collectively, the data point to a scenario where Ca^{2+}-independent binding of the second EF-hand domain further strengthens the association and facilitates the Ca^{2+}-dependent association of the first EF-hand domain (Figure 6A). This latter binding imposes the regulatory mechanism for M1R function and results in a displacement of $G\alpha q_{11}$ from the I3 loop that is controlled by $[Ca^{2+}]_i$ (Figure 6A). $G\alpha q$ coupling requires multipoint contacts in the core of TMDs of GPCR, but early work has already shown that the N-terminal junction of the I3 loop of GPCR plays a role in the coupling process and

specificity of G-protein binding.[137–143] Calneuron-1 binds to the I3 loop at two different sites, and the Ca^{2+}-dependent interaction of the first EF-hand domain overlaps with the binding interface of Gαq and will thereby regulate G-protein coupling via steric hindrance.

The Ca^{2+}-sensing module provided by calneuron-1, the first EF-hand domain, exhibits a global K_D of 230 nM for Ca^{2+}-binding[69,72] and can directly feed back relatively small changes in Ca^{2+}-oscillations close to resting $[Ca^{2+}]_i$ to M1R signaling. Calneuron-1 might thereby integrate $[Ca^{2+}]_i$-transients triggered by various stimuli distant from the receptor to fine-tune M1R downstream signaling and control the timing of M1R activation dependent on $[Ca^{2+}]_i$. Of note, the Ca^{2+}-independent pre-association allows an instantaneous shut-off of M1R-induced G-protein signaling and limits activation of M1R to a very narrow range of $[Ca^{2+}]_i$. In addition, it likely limits an agonist-independent association of G-proteins and constitutive GPCR signaling.

The tight association of calneuron-1 with M1R is likely to play a role in SCZ

Multiple studies suggest that cholinergic signaling is disrupted in SCZ patients and in animal models of SCZ.[106–109,144–146] Muscarinic receptor antagonists exacerbate cognitive deficits and negative symptoms in SCZ patients,[147] whereas the agonist xanomeline reduces all symptom clusters in SCZ patients[66,119] and correspondingly in animal models.[122,148] As outlined above, our data suggest that at least part of the beneficial effects of xanomeline is due to an interruption of the interaction of calneuron-1 and M1R. Xanomeline exhibits properties of an orthosteric and allosteric agonist with two binding sites.[149] Wash-resistant xanomeline binding elicits full long-term receptor activation at M1R and M4R,[149] and we speculate that wash-resistant allosteric binding, which distinguishes xanomeline from other agonists and Cch, is responsible for the long-lasting interruption of the calneuron-1/M1R association (Figure 6B).

M1Rs are the most abundant muscarinic receptors in the HP and PFC, and several studies have shown that they play a crucial role in synaptic plasticity, learning, and memory.[150] Current evidence on how M1R regulates circuits in the PFC that are affected in SCZ suggests regulation of top-down cortical circuits as well as the excitability of the principal cortical output neurons.[150] At present we can only speculate how elevated calneuron-1 levels will interfere with this circuitry. Our data indicate a comparable scenario of task-independent alterations in inhibitory and excitatory neuronal activity in the mPFC. Resulting changes in feed-forward and feedback regulation might lead to impaired local network synchronization and dysfunctional connectivity within the HP-PFC circuitry that was shown to be present already early in life and to underlie later cognitive impairments in SCZ.[92,101,104,151,152] Spatial transcriptomics suggest calneuron-1 expression might be upregulated in neurons of layers 2/3 of the dlPFC in SCZ patients[84,85] like it was observed in mouse models of SCZ in this study. A detailed analysis of changes in local PFC circuitry in response to increased expression of calneuron-1 in neuronal subtypes is ultimately warranted but technically very challenging. Synaptic deficits likely could underlie the deficits in HP-PFC communication, and future work should clarify whether and how, for instance, impairment in muscarinergic LTD is related to SCZ-related abnormalities in excitability and network oscillations.

CALN1 is an SCZ-risk gene

While GWAS support a role of the human *CALN1* gene in SCZ, they do not reveal the underlying mechanisms of calneuron-1 function. A study from the Schizophrenia Working Group of the PGC3 suggested that the CpG island located in the *CALN1* gene promoter is hypermethylated in schizophrenic patients.[153] While there is evidence that the expression of calneuron-1 is positively regulated by DNA methylation, which is as such very uncommon, it appears that at least in the nucleus accumbens DNA methylation interrupts intergenic looping with autism-candidate 2 (*Auts2*), a gene involved in autism-spectrum disorders, and the interruption of intergenic looping results in enhanced gene transcription of calneuron-1 and might be associated with cocaine addiction.[154] It is therefore tempting to speculate that DNA methylation has a causal role for increased *CALN1* gene expression in SCZ. A major problem of GWAS is that common genetic variants typically have minor, if any, effects on disease risk. This highlights the difficulty of deciphering biological effects from hundreds of risk variants of disparate function, scattered across the genome. SCZ-associated risk single-nucleotide polymorphisms identified by GWAS are highly enriched in *cis* regulatory elements, including promoters and enhancers, and frequently regulate the expression of one or more target genes as *cis*- or *trans*-acting expression quantitative trait loci. Whether *CALN1* belongs to such trait loci remains to be determined, but it is conceivable that upregulation of expression is a more common feature of the molecular pathology of SCZ.

RESOURCE AVAILABILITY

Lead contact

Requests for further information and resources should be directed to and will be fulfilled by the lead contact, Michael R. Kreutz (michael.kreutz@lin-magdeburg.de).

Materials availability

This study did not generate new, unique reagents.

Data and code availability

- Data reported in this paper will be shared by the lead contact upon specific request.
- All original code has been deposited at G-Node and is publicly available at 10.12751/g-node.f3z6xr as of the date of publication.
- Additional information required to reanalyze the data reported in this paper is available from the lead contact upon request.

ACKNOWLEDGMENTS

We thank Corinna Borutzki, Isabel Herbert, Monika Marude, Peter Kolch, Achim Dahlmann, Peggy Putthoff, and Annette Marquardt for excellent technical assistance. We want to particularly acknowledge the patients and the Biobank at the Galicia Sur Health Research Institute, the Navarrabiomed Brain Bank, and the Netherlands Brain Bank for their collaboration. Furthermore, we thank Guilherme Gomes and Max Hopf for their support with sample acquisition, processing, or analysis. This work was supported by the German Research Foundation CRC1436 (A03 to S.R.; A02 to A.K.; and A02, A04, and Z01 to M.R.K.), RTG2413 SynAGE (to M.R.K. and S.R.), and FOR5228 (RP06 to A.K. and M.R.K. and RP04 to M.M.); Ha4466/11-1, Ha4466/20-1,

and Ha4466/22-1 to I.H.-O.; DFG Excellence Strategy (EXC-2049–390688087) and the DFG CRC1315 A10 to M.M.; European Research Council 2015-CoG 681577 to I.H.-O.; Horizon 2020 DEEPER 101016787 to I.H.-O.; MSCA-ITN 860563 to I.H.-O.; DAAD postdoctoral fellowship to G.S.; and Leibniz Best Minds StartUp grant (J143/2022) and Swedish Research Council (project 2017-06254) to S.M.; S.R., S.M., and M.R.K. were supported by BMBF/DLR (DZPG, project 01EE2305E).

AUTHOR CONTRIBUTIONS

J.H., A.M.O., J.A.P., and A.R. contributed equally to this work. A.M.O., M.M., S.R., I.H.-O., A.K., and M.R.K. designed the experiments. J.H., A.M.O., J.A.P., A.R., P.P.R., G.N., I.R.-R., P.Y., L.S., H.K., G.S., M.A.-A., A.G., J.L.-R., A.A.A.A., Z.X., and A.K. performed experiments and analyzed data together with P.B. and S.M.; J.H., A.M.O., J.A.P., A.R., and A.K. prepared the figures; and M.R.K. conceptualized the study and wrote the manuscript together with A.M.O., J.A.P., I.H.-O., and A.K. All authors read and commented on the manuscript.

DECLARATION OF INTERESTS

The authors declare no competing interests.

STAR★METHODS

Detailed methods are provided in the online version of this paper and include the following:

- KEY RESOURCES TABLE
- EXPERIMENTAL MODEL AND SUBJECT DETAILS
  - Animals
  - Human brain samples
- METHOD DETAILS
  - Quantitative real-time PCR
  - RNAscope
  - Quantitative immunoblot analysis of human brain tissue
  - Protein extraction from transfected HEK293T cells and immunoprecipitation
  - Expression and purification of bacterially produced recombinant proteins
  - Pull-down experiments
  - Surface plasmon resonance
  - Cell culture and transfection
  - FRET assay
  - Human i3-iPSCs derived neurons
  - Immunocytochemistry, immunohistochemistry and proximity ligation assay
  - Confocal Laser Scanning Microscopy and Image Analysis
  - Viral constructs and viral particle production
  - Lentiviral knockdown of calneuron-1 in rat striatal primary cultures
  - mPFC slice preparation and fEPSP recording
  - Miniature inhibitory postsynaptic current (mIPSC) recordings in coronal brain slices and striatal primary neurons
  - *In vivo* recordings in mice overexpressing calneuron-1 developmentally
  - In vivo recordings in mice overexpressing calneuron-1 in adulthood
  - Analysis of electrophysiological data
  - Behavioral tests

SUPPLEMENTAL INFORMATION

Supplemental information can be found online at https://doi.org/10.1016/j.neuron.2025.10.038.

Received: August 12, 2024
Revised: August 1, 2025
Accepted: October 30, 2025

REFERENCES

1. Singh, T., Walters, J.T.R., Johnstone, M., Curtis, D., Suvisaari, J., Torniainen, M., Rees, E., Iyegbe, C., Blackwood, D., McIntosh, A.M., et al. (2017). The contribution of rare variants to risk of schizophrenia in individuals with and without intellectual disability. Nat. Genet. *49*, 1167–1173. https://doi.org/10.1038/ng.3903.

2. Rees, E., Han, J., Morgan, J., Carrera, N., Escott-Price, V., Pocklington, A.J., Duffield, M., Hall, L.S., Legge, S.E., Pardiñas, A.F., et al. (2020). De novo mutations identified by exome sequencing implicate rare missense variants in SLC6A1 in schizophrenia. Nat. Neurosci. *23*, 179–184. https://doi.org/10.1038/s41593-019-0565-2.

3. Pocklington, A.J., Rees, E., Walters, J.T.R., Han, J., Kavanagh, D.H., Chambert, K.D., Holmans, P., Moran, J.L., McCarroll, S.A., Kirov, G., et al. (2015). Novel Findings from CNVs Implicate Inhibitory and Excitatory Signaling Complexes in Schizophrenia. Neuron *86*, 1203–1214. https://doi.org/10.1016/j.neuron.2015.04.022.

4. Lam, M., Chen, C.Y., Li, Z., Martin, A.R., Bryois, J., Ma, X., Gaspar, H., Ikeda, M., Benyamin, B., Brown, B.C., et al. (2019). Comparative genetic architectures of schizophrenia in East Asian and European populations. Nat. Genet. *51*, 1670–1678. https://doi.org/10.1038/s41588-019-0512-x.

5. International; Schizophrenia Consortium, Purcell, S.M., Wray, N.R., Stone, J.L., Visscher, P.M., O'Donovan, M.C., Sullivan, P.F., and Sklar, P. (2009). Common polygenic variation contributes to risk of schizophrenia and bipolar disorder. Nature *460*, 748–752. https://doi.org/10.1038/nature08185.

6. Devaraju, P., Yu, J., Eddins, D., Mellado-Lagarde, M.M., Earls, L.R., Westmoreland, J.J., Quarato, G., Green, D.R., and Zakharenko, S.S. (2017). Haploinsufficiency of the 22q11.2 microdeletion gene Mrpl40 disrupts short-term synaptic plasticity and working memory through dysregulation of mitochondrial calcium. Mol. Psychiatry *22*, 1313–1326. https://doi.org/10.1038/mp.2016.75.

7. Devaraju, P., and Zakharenko, S.S. (2017). Mitochondria in complex psychiatric disorders: Lessons from mouse models of 22q11.2 deletion syndrome: Hemizygous deletion of several mitochondrial genes in the 22q11.2 genomic region can lead to symptoms associated with neuropsychiatric disease. BioEssays *39*. https://doi.org/10.1002/bies.201600177.

8. Fénelon, K., Mukai, J., Xu, B., Hsu, P.K., Drew, L.J., Karayiorgou, M., Fischbach, G.D., Macdermott, A.B., and Gogos, J.A. (2011). Deficiency of Dgcr8, a gene disrupted by the 22q11.2 microdeletion, results in altered short-term plasticity in the prefrontal cortex. Proc. Natl. Acad. Sci. USA *108*, 4447–4452. https://doi.org/10.1073/pnas.1101219108.

9. Fernandez, A., Meechan, D.W., Karpinski, B.A., Paronett, E.M., Bryan, C.A., Rutz, H.L., Radin, E.A., Lubin, N., Bonner, E.R., Popratiloff, A., et al. (2019). Mitochondrial Dysfunction Leads to Cortical Under-Connectivity and Cognitive Impairment. Neuron *102*, 1127–1142.e3. https://doi.org/10.1016/j.neuron.2019.04.013.

10. Khan, T.A., Revah, O., Gordon, A., Yoon, S.J., Krawisz, A.K., Goold, C., Sun, Y., Kim, C.H., Tian, Y., Li, M.Y., et al. (2020). Neuronal defects in a human cellular model of 22q11.2 deletion syndrome. Nat. Med. *26*, 1888–1898. https://doi.org/10.1038/s41591-020-1043-9.

11. Li, J., Ryan, S.K., Deboer, E., Cook, K., Fitzgerald, S., Lachman, H.M., Wallace, D.C., Goldberg, E.M., and Anderson, S.A. (2019). Mitochondrial deficits in human iPSC-derived neurons from patients with 22q11.2 deletion syndrome and schizophrenia. Transl. Psychiatry *9*, 302. https://doi.org/10.1038/s41398-019-0643-y.

12. Li, J., Tran, O.T., Crowley, T.B., Moore, T.M., Zackai, E.H., Emanuel, B.S., McDonald-McGinn, D.M., Gur, R.E., Wallace, D.C., and Anderson, S.A. (2021). Association of Mitochondrial Biogenesis With Variable Penetrance of Schizophrenia. JAMA Psychiatry *78*, 911–921. https://doi.org/10.1001/jamapsychiatry.2021.0762.

13. Nehme, R., Pietiläinen, O., Artomov, M., Tegtmeyer, M., Valakh, V., Lehtonen, L., Bell, C., Singh, T., Trehan, A., Sherwood, J., et al. (2022). The 22q11.2 region regulates presynaptic gene-products linked to schizophrenia. Nat. Commun. *13*, 3690. https://doi.org/10.1038/s41467-022-31436-8.

14. Duan, X., Chang, J.H., Ge, S., Faulkner, R.L., Kim, J.Y., Kitabatake, Y., Liu, X.B., Yang, C.H., Jordan, J.D., Ma, D.K., et al. (2007). Disrupted-In-Schizophrenia 1 regulates integration of newly generated neurons in the adult brain. Cell *130*, 1146–1158. https://doi.org/10.1016/j.cell.2007.07.010.

15. Kim, J.Y., Duan, X., Liu, C.Y., Jang, M.H., Guo, J.U., Pow-anpongkul, N., Kang, E., Song, H., and Ming, G.L. (2009). DISC1 regulates new neuron development in the adult brain via modulation of AKT-mTOR signaling through KIAA1212. Neuron *63*, 761–773. https://doi.org/10.1016/j.neuron.2009.08.008.

16. Kim, J.Y., Liu, C.Y., Zhang, F., Duan, X., Wen, Z., Song, J., Feighery, E., Lu, B., Rujescu, D., St Clair, D., et al. (2012). Interplay between DISC1 and GABA signaling regulates neurogenesis in mice and risk for schizophrenia. Cell *148*, 1051–1064. https://doi.org/10.1016/j.cell.2011.12.037.

17. Mao, Y., Ge, X., Frank, C.L., Madison, J.M., Koehler, A.N., Doud, M.K., Tassa, C., Berry, E.M., Soda, T., Singh, K.K., et al. (2009). Disrupted in schizophrenia 1 regulates neuronal progenitor proliferation via modulation of GSK3beta/beta-catenin signaling. Cell *136*, 1017–1031. https://doi.org/10.1016/j.cell.2008.12.044.

18. Hayashi-Takagi, A., Takaki, M., Graziane, N., Seshadri, S., Murdoch, H., Dunlop, A.J., Makino, Y., Seshadri, A.J., Ishizuka, K., Srivastava, D.P., et al. (2010). Disrupted-in-Schizophrenia 1 (DISC1) regulates spines of the glutamate synapse via Rac1. Nat. Neurosci. *13*, 327–332. https://doi.org/10.1038/nn.2487.

19. Kvajo, M., McKellar, H., Arguello, P.A., Drew, L.J., Moore, H., MacDermott, A.B., Karayiorgou, M., and Gogos, J.A. (2008). A mutation in mouse Disc1 that models a schizophrenia risk allele leads to specific alterations in neuronal architecture and cognition. Proc. Natl. Acad. Sci. USA *105*, 7076–7081. https://doi.org/10.1073/pnas.0802615105.

20. Kvajo, M., McKellar, H., Drew, L.J., Lepagnol-Bestel, A.M., Xiao, L., Levy, R.J., Blazeski, R., Arguello, P.A., Lacefield, C.O., Mason, C.A., et al. (2011). Altered axonal targeting and short-term plasticity in the hippocampus of Disc1 mutant mice. Proc. Natl. Acad. Sci. USA *108*, E1349–E1358. https://doi.org/10.1073/pnas.1114113108.

21. Malavasi, E.L.V., Economides, K.D., Grünewald, E., Makedonopoulou, P., Gautier, P., Mackie, S., Murphy, L.C., Murdoch, H., Crummie, D., Ogawa, F., et al. (2018). DISC1 regulates N-methyl-D-aspartate receptor dynamics: abnormalities induced by a Disc1 mutation modelling a translocation linked to major mental illness. Transl. Psychiatry *8*, 184. https://doi.org/10.1038/s41398-018-0228-1.

22. Hikida, T., Jaaro-Peled, H., Seshadri, S., Oishi, K., Hookway, C., Kong, S., Wu, D., Xue, R., Andradé, M., Tankou, S., et al. (2007). Dominant-negative DISC1 transgenic mice display schizophrenia-associated phenotypes detected by measures translatable to humans. Proc. Natl. Acad. Sci. USA *104*, 14501–14506. https://doi.org/10.1073/pnas.0704774104.

23. Jaaro-Peled, H., Niwa, M., Foss, C.A., Murai, R., de Los Reyes, S., Kamiya, A., Mateo, Y., O'Donnell, P., Cascella, N.G., Nabeshima, T., et al. (2013). Subcortical dopaminergic deficits in a DISC1 mutant model: a study in direct reference to human molecular brain imaging. Hum. Mol. Genet. *22*, 1574–1580. https://doi.org/10.1093/hmg/ddt007.

24. Niwa, M., Jaaro-Peled, H., Tankou, S., Seshadri, S., Hikida, T., Matsumoto, Y., Cascella, N.G., Kano, S., Ozaki, N., Nabeshima, T., et al. (2013). Adolescent stress-induced epigenetic control of dopaminergic neurons via glucocorticoids. Science *339*, 335–339. https://doi.org/10.1126/science.1226931.

25. Niwa, M., Kamiya, A., Murai, R., Kubo, K., Gruber, A.J., Tomita, K., Lu, L., Tomisato, S., Jaaro-Peled, H., Seshadri, S., et al. (2010). Knockdown of DISC1 by in utero gene transfer disturbs postnatal dopaminergic maturation in the frontal cortex and leads to adult behavioral deficits. Neuron *65*, 480–489. https://doi.org/10.1016/j.neuron.2010.01.019.

26. Su, P., Li, S., Chen, S., Lipina, T.V., Wang, M., Lai, T.K.Y., Lee, F.H.F., Zhang, H., Zhai, D., Ferguson, S.S.G., et al. (2014). A dopamine D2 receptor-DISC1 protein complex may contribute to antipsychotic-like effects. Neuron *84*, 1302–1316. https://doi.org/10.1016/j.neuron.2014.11.007.

27. Trossbach, S.V., Bader, V., Hecher, L., Pum, M.E., Masoud, S.T., Prikulis, I., Schäble, S., de Souza Silva, M.A., Su, P., Boulat, B., et al. (2016). Misassembly of full-length Disrupted-in-Schizophrenia 1 protein is linked to altered dopamine homeostasis and behavioral deficits. Mol. Psychiatry *21*, 1561–1572. https://doi.org/10.1038/mp.2015.194.

28. Park, S.J., Lee, S.B., Suh, Y., Kim, S.J., Lee, N., Hong, J.H., Park, C., Woo, Y., Ishizuka, K., Kim, J.H., et al. (2017). DISC1 Modulates Neuronal Stress Responses by Gate-Keeping ER-Mitochondria Ca(2+) Transfer through the MAM. Cell Rep. *21*, 2748–2759. https://doi.org/10.1016/j.celrep.2017.11.043.

29. Park, Y.U., Jeong, J., Lee, H., Mun, J.Y., Kim, J.H., Lee, J.S., Nguyen, M.D., Han, S.S., Suh, P.G., and Park, S.K. (2010). Disrupted-in-schizophrenia 1 (DISC1) plays essential roles in mitochondria in collaboration with Mitofilin. Proc. Natl. Acad. Sci. USA *107*, 17785–17790. https://doi.org/10.1073/pnas.1004361107.

30. Chen, Y.J., Zhang, M., Yin, D.M., Wen, L., Ting, A., Wang, P., Lu, Y.S., Zhu, X.H., Li, S.J., Wu, C.Y., et al. (2010). ErbB4 in parvalbumin-positive interneurons is critical for neuregulin 1 regulation of long-term potentiation. Proc. Natl. Acad. Sci. USA *107*, 21818–21823. https://doi.org/10.1073/pnas.1010669107.

31. Del Pino, I., García-Frigola, C., Dehorter, N., Brotons-Mas, J.R., Alvarez-Salvado, E., Martínez de Lagrán, M., Ciceri, G., Gabaldón, M.V., Moratal, D., Dierssen, M., et al. (2013). Erbb4 deletion from fast-spiking interneurons causes schizophrenia-like phenotypes. Neuron *79*, 1152–1168. https://doi.org/10.1016/j.neuron.2013.07.010.

32. Dong, J., Chen, W., Liu, N., Chang, S., Zhu, W., and Kang, J. (2022). NRG1 knockdown rescues PV interneuron GABAergic maturation deficits and schizophrenia behaviors in fetal growth restriction mice. Cell Death Discov. *8*, 476. https://doi.org/10.1038/s41420-022-01271-3.

33. Fazzari, P., Paternain, A.V., Valiente, M., Pla, R., Luján, R., Lloyd, K., Lerma, J., Marín, O., and Rico, B. (2010). Control of cortical GABA circuitry development by Nrg1 and ErbB4 signalling. Nature *464*, 1376–1380. https://doi.org/10.1038/nature08928.

34. Flames, N., Long, J.E., Garratt, A.N., Fischer, T.M., Gassmann, M., Birchmeier, C., Lai, C., Rubenstein, J.L.R., and Marín, O. (2004). Short- and long-range attraction of cortical GABAergic interneurons by neuregulin-1. Neuron *44*, 251–261. https://doi.org/10.1016/j.neuron.2004.09.028.

35. Law, A.J., Kleinman, J.E., Weinberger, D.R., and Weickert, C.S. (2007). Disease-associated intronic variants in the ErbB4 gene are related to altered ErbB4 splice-variant expression in the brain in schizophrenia. Hum. Mol. Genet. *16*, 129–141. https://doi.org/10.1093/hmg/ddl449.

36. Marenco, S., Geramita, M., van der Veen, J.W., Barnett, A.S., Kolachana, B., Shen, J., Weinberger, D.R., and Law, A.J. (2011). Genetic association of ErbB4 and human cortical GABA levels in vivo. J. Neurosci. *31*, 11628–11632. https://doi.org/10.1523/JNEUROSCI.1529-11.2011.

37. Mitchell, R.M., Janssen, M.J., Karavanova, I., Vullhorst, D., Furth, K., Makusky, A., Markey, S.P., and Buonanno, A. (2013). ErbB4 reduces synaptic GABAA currents independent of its receptor tyrosine kinase activity. Proc. Natl. Acad. Sci. USA *110*, 19603–19608. https://doi.org/10.1073/pnas.1312791110.

38. Mostaid, M.S., Mancuso, S.G., Liu, C., Sundram, S., Pantelis, C., Everall, I.P., and Bousman, C.A. (2017). Meta-analysis reveals associations between genetic variation in the 5′ and 3′ regions of Neuregulin-1 and schizophrenia. Transl. Psychiatry *7*, e1004. https://doi.org/10.1038/tp.2016.279.

39. Stefansson, H., Sarginson, J., Kong, A., Yates, P., Steinthorsdottir, V., Gudfinnsson, E., Gunnarsdottir, S., Walker, N., Petursson, H., Crombie, C., et al. (2003). Association of neuregulin 1 with schizophrenia confirmed in a Scottish population. Am. J. Hum. Genet. *72*, 83–87. https://doi.org/10.1086/345442.

40. Sun, Y., Ikrar, T., Davis, M.F., Gong, N., Zheng, X., Luo, Z.D., Lai, C., Mei, L., Holmes, T.C., Gandhi, S.P., et al. (2016). Neuregulin-1/ErbB4 Signaling Regulates Visual Cortical Plasticity. Neuron *92*, 160–173. https://doi.org/10.1016/j.neuron.2016.08.033.

41. Wang, Y.Y., Zhao, B., Wu, M.M., Zheng, X.L., Lin, L., and Yin, D.M. (2021). Overexpression of neuregulin 1 in GABAergic interneurons results in reversible cortical disinhibition. Nat. Commun. *12*, 278. https://doi.org/10.1038/s41467-020-20552-y.

42. Wen, L., Lu, Y.S., Zhu, X.H., Li, X.M., Woo, R.S., Chen, Y.J., Yin, D.M., Lai, C., Terry, A.V., Jr., Vazdarjanova, A., et al. (2010). Neuregulin 1 regulates pyramidal neuron activity via ErbB4 in parvalbumin-positive interneurons. Proc. Natl. Acad. Sci. USA *107*, 1211–1216. https://doi.org/10.1073/pnas.0910302107.

43. Bertolino, A., Caforio, G., Blasi, G., De Candia, M., Latorre, V., Petruzzella, V., Altamura, M., Nappi, G., Papa, S., Callicott, J.H., et al. (2004). Interaction of COMT (Val(108/158)Met) genotype and olanzapine treatment on prefrontal cortical function in patients with schizophrenia. Am. J. Psychiatry *161*, 1798–1805. https://doi.org/10.1176/ajp.161.10.1798.

44. Chen, J., Lipska, B.K., Halim, N., Ma, Q.D., Matsumoto, M., Melhem, S., Kolachana, B.S., Hyde, T.M., Herman, M.M., Apud, J., et al. (2004). Functional analysis of genetic variation in catechol-O-methyltransferase (COMT): effects on mRNA, protein, and enzyme activity in postmortem human brain. Am. J. Hum. Genet. *75*, 807–821. https://doi.org/10.1086/425589.

45. Egan, M.F., Goldberg, T.E., Kolachana, B.S., Callicott, J.H., Mazzanti, C.M., Straub, R.E., Goldman, D., and Weinberger, D.R. (2001). Effect of COMT Val108/158 Met genotype on frontal lobe function and risk for schizophrenia. Proc. Natl. Acad. Sci. USA *98*, 6917–6922. https://doi.org/10.1073/pnas.111134598.

46. Käenmäki, M., Tammimäki, A., Myöhänen, T., Pakarinen, K., Amberg, C., Karayiorgou, M., Gogos, J.A., and Männistö, P.T. (2010). Quantitative role of COMT in dopamine clearance in the prefrontal cortex of freely moving mice. J. Neurochem. *114*, 1745–1755. https://doi.org/10.1111/j.1471-4159.2010.06889.x.

47. Mattay, V.S., Goldberg, T.E., Fera, F., Hariri, A.R., Tessitore, A., Egan, M.F., Kolachana, B., Callicott, J.H., and Weinberger, D.R. (2003). Catechol O-methyltransferase val158-met genotype and individual variation in the brain response to amphetamine. Proc. Natl. Acad. Sci. USA *100*, 6186–6191. https://doi.org/10.1073/pnas.0931309100.

48. Meyer-Lindenberg, A., Kohn, P.D., Kolachana, B., Kippenhan, S., McInerney-Leo, A., Nussbaum, R., Weinberger, D.R., and Berman, K.F. (2005). Midbrain dopamine and prefrontal function in humans: interaction and modulation by COMT genotype. Nat. Neurosci. *8*, 594–596. https://doi.org/10.1038/nn1438.

49. Shifman, S., Bronstein, M., Sternfeld, M., Pisanté-Shalom, A., Lev-Lehman, E., Weizman, A., Reznik, I., Spivak, B., Grisaru, N., Karp, L., et al. (2002). A highly significant association between a COMT haplotype and schizophrenia. Am. J. Hum. Genet. *71*, 1296–1302. https://doi.org/10.1086/344514.

50. Slifstein, M., Kolachana, B., Simpson, E.H., Tabares, P., Cheng, B., Duvall, M., Frankle, W.G., Weinberger, D.R., Laruelle, M., and Abi-Dargham, A. (2008). COMT genotype predicts cortical-limbic D1 receptor availability measured with [11C]NNC112 and PET. Mol. Psychiatry *13*, 821–827. https://doi.org/10.1038/mp.2008.19.

51. Tunbridge, E.M., Bannerman, D.M., Sharp, T., and Harrison, P.J. (2004). Catechol-o-methyltransferase inhibition improves set-shifting performance and elevates stimulated dopamine release in the rat prefrontal cortex. J. Neurosci. *24*, 5331–5335. https://doi.org/10.1523/JNEUROSCI.1124-04.2004.

52. Yavich, L., Forsberg, M.M., Karayiorgou, M., Gogos, J.A., and Männistö, P.T. (2007). Site-specific role of catechol-O-methyltransferase in dopamine overflow within prefrontal cortex and dorsal striatum. J. Neurosci. *27*, 10196–10209. https://doi.org/10.1523/JNEUROSCI.0665-07.2007.

53. Hall, J., and Bray, N.J. (2022). Schizophrenia Genomics: Convergence on Synaptic Development, Adult Synaptic Plasticity, or Both? Biol. Psychiatry *91*, 709–717. https://doi.org/10.1016/j.biopsych.2021.10.018.

54. Fromer, M., Pocklington, A.J., Kavanagh, D.H., Williams, H.J., Dwyer, S., Gormley, P., Georgieva, L., Rees, E., Palta, P., Ruderfer, D.M., et al. (2014). De novo mutations in schizophrenia implicate synaptic networks. Nature *506*, 179–184. https://doi.org/10.1038/nature12929.

55. Singh, T., Poterba, T., Curtis, D., Akil, H., Al Eissa, M., Barchas, J.D., Bass, N., Bigdeli, T.B., Breen, G., Bromet, E.J., et al. (2022). Rare coding variants in ten genes confer substantial risk for schizophrenia. Nature *604*, 509–516. https://doi.org/10.1038/s41586-022-04556-w.

56. Cross-Disorder Group of the Psychiatric; Genomics Consortium (2013). Identification of risk loci with shared effects on five major psychiatric disorders: a genome-wide analysis. Lancet *381*, 1371–1379. https://doi.org/10.1016/S0140-6736(12)62129-1.

57. Datta, D., Yang, S., Joyce, M.K.P., Woo, E., McCarroll, S.A., Gonzalez-Burgos, G., Perone, I., Uchendu, S., Ling, E., Goldman, M., et al. (2024). Key Roles of CACNA1C/Cav1.2 and CALB1/Calbindin in Prefrontal Neurons Altered in Cognitive Disorders. JAMA Psychiatry *81*, 870–881. https://doi.org/10.1001/jamapsychiatry.2024.1112.

58. O'Donovan, M.C., Craddock, N., Norton, N., Williams, H., Peirce, T., Moskvina, V., Nikolov, I., Hamshere, M., Carroll, L., Georgieva, L., et al. (2008). Identification of loci associated with schizophrenia by genome-wide association and follow-up. Nat. Genet. *40*, 1053–1055. https://doi.org/10.1038/ng.201.

59. Yilmaz, M., Yalcin, E., Presumey, J., Aw, E., Ma, M., Whelan, C.W., Stevens, B., McCarroll, S.A., and Carroll, M.C. (2021). Overexpression of schizophrenia susceptibility factor human complement C4A promotes excessive synaptic loss and behavioral changes in mice. Nat. Neurosci. *24*, 214–224. https://doi.org/10.1038/s41593-020-00763-8.

60. Ghoshal, A., Rook, J.M., Dickerson, J.W., Roop, G.N., Morrison, R.D., Jalan-Sakrikar, N., Lamsal, A., Noetzel, M.J., Poslusney, M.S., Wood, M.R., et al. (2016). Potentiation of M1 Muscarinic Receptor Reverses Plasticity Deficits and Negative and Cognitive Symptoms in a Schizophrenia Mouse Model. Neuropsychopharmacology *41*, 598–610. https://doi.org/10.1038/npp.2015.189.

61. Manoach, D.S. (2003). Prefrontal cortex dysfunction during working memory performance in schizophrenia: reconciling discrepant findings. Schizophr. Res. *60*, 285–298. https://doi.org/10.1016/s0920-9964(02)00294-3.

62. Moran, S.P., Maksymetz, J., and Conn, P.J. (2019). Targeting Muscarinic Acetylcholine Receptors for the Treatment of Psychiatric and Neurological Disorders. Trends Pharmacol. Sci. *40*, 1006–1020. https://doi.org/10.1016/j.tips.2019.10.007.

63. Raedler, T.J., Bymaster, F.P., Tandon, R., Copolov, D., and Dean, B. (2007). Towards a muscarinic hypothesis of schizophrenia. Mol. Psychiatry *12*, 232–246. https://doi.org/10.1038/sj.mp.4001924.

64. Caruana, D.A., Warburton, E.C., and Bashir, Z.I. (2011). Induction of activity-dependent LTD requires muscarinic receptor activation in medial prefrontal cortex. J. Neurosci. *31*, 18464–18478. https://doi.org/10.1523/JNEUROSCI.4719-11.2011.

65. Strube, W., Bunse, T., Nitsche, M.A., Wobrock, T., Aborowa, R., Misewitsch, K., Herrmann, M., Falkai, P., and Hasan, A. (2015). Smoking restores impaired LTD-like plasticity in schizophrenia: a transcranial direct current stimulation study. Neuropsychopharmacology *40*, 822–830. https://doi.org/10.1038/npp.2014.275.

66. Kaul, I., Sawchak, S., Walling, D.P., Tamminga, C.A., Breier, A., Zhu, H., Miller, A.C., Paul, S.M., and Brannan, S.K. (2024). Efficacy and Safety of Xanomeline-Trospium Chloride in Schizophrenia: A Randomized Clinical Trial. JAMA Psychiatry *81*, 749–756. https://doi.org/10.1001/jamapsychiatry.2024.0785.

67. Mikhaylova, M., Hradsky, J., and Kreutz, M.R. (2011). Between promiscuity and specificity: novel roles of EF-hand calcium sensors in neuronal Ca2+ signalling. J. Neurochem. *118*, 695–713. https://doi.org/10.1111/j.1471-4159.2011.07372.x.

68. Mikhaylova, M., Reddy, P.P., and Kreutz, M.R. (2010). Role of neuronal Ca2+-sensor proteins in Golgi-cell-surface membrane traffic. Biochem. Soc. Trans. *38*, 177–180. https://doi.org/10.1042/BST0380177.

69. Mikhaylova, M., Sharma, Y., Reissner, C., Nagel, F., Aravind, P., Rajini, B., Smalla, K.H., Gundelfinger, E.D., and Kreutz, M.R. (2006). Neuronal Ca2+ signaling via caldendrin and calneurons. Biochim. Biophys. Acta *1763*, 1229–1237. https://doi.org/10.1016/j.bbamcr.2006.08.047.

70. Wu, Y.Q., Lin, X., Liu, C.M., Jamrich, M., and Shaffer, L.G. (2001). Identification of a human brain-specific gene, calneuron 1, a new member of the calmodulin superfamily. Mol. Genet. Metab. *72*, 343–350. https://doi.org/10.1006/mgme.2001.3160.

71. Hradsky, J., Raghuram, V., Reddy, P.P., Navarro, G., Hupe, M., Casado, V., McCormick, P.J., Sharma, Y., Kreutz, M.R., and Mikhaylova, M. (2011). Post-translational membrane insertion of tail-anchored transmembrane EF-hand Ca2+ sensor calneurons requires the TRC40/Asna1 protein chaperone. J. Biol. Chem. *286*, 36762–36776. https://doi.org/10.1074/jbc.M111.280339.

72. Mikhaylova, M., Reddy, P.P., Munsch, T., Landgraf, P., Suman, S.K., Smalla, K.H., Gundelfinger, E.D., Sharma, Y., and Kreutz, M.R. (2009). Calneurons provide a calcium threshold for trans-Golgi network to plasma membrane trafficking. Proc. Natl. Acad. Sci. USA *106*, 9093–9098. https://doi.org/10.1073/pnas.0903001106.

73. Roussos, P., Giakoumaki, S.G., Zouraraki, C., Fullard, J.F., Karagiorga, V.E., Tsapakis, E.M., Petraki, Z., Siever, L.J., Lencz, T., Malhotra, A., et al. (2016). The Relationship of Common Risk Variants and Polygenic Risk for Schizophrenia to Sensorimotor Gating. Biol. Psychiatry *79*, 988–996. https://doi.org/10.1016/j.biopsych.2015.06.019.

74. Li, Z., Xiang, Y., Chen, J., Li, Q., Shen, J., Liu, Y., Li, W., Xing, Q., Wang, Q., Wang, L., et al. (2015). Loci with genome-wide associations with schizophrenia in the Han Chinese population. Br. J. Psychiatry *207*, 490–494. https://doi.org/10.1192/bjp.bp.114.150490.

75. Lam, M., Hill, W.D., Trampush, J.W., Yu, J., Knowles, E., Davies, G., Stahl, E., Huckins, L., Liewald, D.C., Djurovic, S., et al. (2019). Pleiotropic Meta-Analysis of Cognition, Education, and Schizophrenia Differentiates Roles of Early Neurodevelopmental and Adult Synaptic Pathways. Am. J. Hum. Genet. *105*, 334–350. https://doi.org/10.1016/j.ajhg.2019.06.012.

76. Ikeda, M., Takahashi, A., Kamatani, Y., Momozawa, Y., Saito, T., Kondo, K., Shimasaki, A., Kawase, K., Sakusabe, T., Iwayama, Y., et al. (2019). Genome-Wide Association Study Detected Novel Susceptibility Genes for Schizophrenia and Shared Trans-Populations/Diseases Genetic Effect. Schizophr. Bull. *45*, 824–834. https://doi.org/10.1093/schbul/sby140.

77. Hamshere, M.L., Walters, J.T., Smith, R., Richards, A.L., Green, E., Grozeva, D., Jones, I., Forty, L., Jones, L., Gordon-Smith, K., et al. (2013). Genome-wide significant associations in schizophrenia to ITIH3/4, CACNA1C and SDCCAG8, and extensive replication of associations reported by the Schizophrenia PGC. Mol. Psychiatry *18*, 708–712. https://doi.org/10.1038/mp.2012.67.

78. Goes, F.S., McGrath, J., Avramopoulos, D., Wolyniec, P., Pirooznia, M., Ruczinski, I., Nestadt, G., Kenny, E.E., Vacic, V., Peters, I., et al. (2015). Genome-wide association study of schizophrenia in Ashkenazi Jews. Am. J. Med. Genet. B Neuropsychiatr. Genet. *168*, 649–659. https://doi.org/10.1002/ajmg.b.32349.

79. Peyrot, W.J., and Price, A.L. (2021). Identifying loci with different allele frequencies among cases of eight psychiatric disorders using CC-GWAS. Nat. Genet. *53*, 445–454. https://doi.org/10.1038/s41588-021-00787-1.

80. Dang, X., Teng, Z., Yang, Y., Li, W., Liu, J., Hui, L., Zhou, D., Gong, D., Dai, S.S., Li, Y., et al. (2025). Gene-level analysis reveals the genetic aetiology and therapeutic targets of schizophrenia. Nat. Hum. Behav. *9*, 609–624. https://doi.org/10.1038/s41562-024-02091-4.

81. Schizophrenia Psychiatric Genome-Wide Association Study (GWAS) Consortium (2011). Genome-wide association study identifies five new schizophrenia loci. Nat. Genet. *43*, 969–976. https://doi.org/10.1038/ng.940.

82. Trubetskoy, V., Pardiñas, A.F., Qi, T., Panagiotaropoulou, G., Awasthi, S., Bigdeli, T.B., Bryois, J., Chen, C.Y., Dennison, C.A., Hall, L.S., et al. (2022). Mapping genomic loci implicates genes and synaptic biology in schizophrenia. Nature *604*, 502–508. https://doi.org/10.1038/s41586-022-04434-5.

83. Ohi, K., Shimada, T., Nitta, Y., Kihara, H., Okubo, H., Uehara, T., and Kawasaki, Y. (2016). Schizophrenia risk variants in ITIH4 and CALN1 regulate gene expression in the dorsolateral prefrontal cortex. Psychiatr. Genet. *26*, 142–143. https://doi.org/10.1097/YPG.0000000000000127.

84. Batiuk, M.Y., Tyler, T., Dragicevic, K., Mei, S., Rydbirk, R., Petukhov, V., Deviatiiarov, R., Sedmak, D., Frank, E., Feher, V., et al. (2022). Upper cortical layer-driven network impairment in schizophrenia. Sci. Adv. *8*, eabn8367. https://doi.org/10.1126/sciadv.abn8367.

85. Fromer, M., Roussos, P., Sieberts, S.K., Johnson, J.S., Kavanagh, D.H., Perumal, T.M., Ruderfer, D.M., Oh, E.C., Topol, A., Shah, H.R., et al. (2016). Gene expression elucidates functional impact of polygenic risk for schizophrenia. Nat. Neurosci. *19*, 1442–1453. https://doi.org/10.1038/nn.4399.

86. Brandon, N.J., and Sawa, A. (2011). Linking neurodevelopmental and synaptic theories of mental illness through DISC1. Nat. Rev. Neurosci. *12*, 707–722. https://doi.org/10.1038/nrn3120.

87. Nilsson, S.R., Fejgin, K., Gastambide, F., Vogt, M.A., Kent, B.A., Nielsen, V., Nielsen, J., Gass, P., Robbins, T.W., Saksida, L.M., et al. (2016). Assessing the Cognitive Translational Potential of a Mouse Model of the 22q11.2 Microdeletion Syndrome. Cereb. Cortex *26*, 3991–4003. https://doi.org/10.1093/cercor/bhw229.

88. Oberlander, V.C., Xu, X., Chini, M., and Hanganu-Opatz, I.L. (2019). Developmental dysfunction of prefrontal-hippocampal networks in mouse models of mental illness. Eur. J. Neurosci. *50*, 3072–3084. https://doi.org/10.1111/ejn.14436.

89. Hartung, H., Cichon, N., De Feo, V., Riemann, S., Schildt, S., Lindemann, C., Mulert, C., Gogos, J.A., and Hanganu-Opatz, I.L. (2016). From Shortage to Surge: A Developmental Switch in Hippocampal-Prefrontal Coupling in a Gene-Environment Model of Neuropsychiatric Disorders. Cereb. Cortex *26*, 4265–4281. https://doi.org/10.1093/cercor/bhw274.

90. Crabtree, G.W., Sun, Z., Kvajo, M., Broek, J.A.C., Fénelon, K., McKellar, H., Xiao, L., Xu, B., Bahn, S., O'Donnell, J.M., et al. (2017). Alteration of Neuronal Excitability and Short-Term Synaptic Plasticity in the Prefrontal Cortex of a Mouse Model of Mental Illness. J. Neurosci. *37*, 4158–4180. https://doi.org/10.1523/JNEUROSCI.4345-15.2017.

91. Koike, H., Arguello, P.A., Kvajo, M., Karayiorgou, M., and Gogos, J.A. (2006). Disc1 is mutated in the 129S6/SvEv strain and modulates working memory in mice. Proc. Natl. Acad. Sci. USA *103*, 3693–3697. https://doi.org/10.1073/pnas.0511189103.

92. Sigurdsson, T., Stark, K.L., Karayiorgou, M., Gogos, J.A., and Gordon, J.A. (2010). Impaired hippocampal-prefrontal synchrony in a genetic mouse model of schizophrenia. Nature *464*, 763–767. https://doi.org/10.1038/nature08855.

93. Rajagopal, L., Massey, B.W., Huang, M., Oyamada, Y., and Meltzer, H.Y. (2014). The novel object recognition test in rodents in relation to cognitive

impairment in schizophrenia. Curr. Pharm. Des. *20*, 5104–5114. https://doi.org/10.2174/1381612819666131216114240.

94. Vaitl, D., Lipp, O., Bauer, U., Schüler, G., Stark, R., Zimmermann, M., and Kirsch, P. (2002). Latent inhibition and schizophrenia: Pavlovian conditioning of autonomic responses. Schizophr. Res. *55*, 147–158. https://doi.org/10.1016/s0920-9964(01)00250-x.

95. Feigenson, K.A., Kusnecov, A.W., and Silverstein, S.M. (2014). Inflammation and the two-hit hypothesis of schizophrenia. Neurosci. Biobehav. Rev. *38*, 72–93. https://doi.org/10.1016/j.neubiorev.2013.11.006.

96. Horváth, S., and Mirnics, K. (2009). Breaking the gene barrier in schizophrenia. Nat. Med. *15*, 488–490. https://doi.org/10.1038/nm0509-488.

97. Schubert, D., Martens, G.J., and Kolk, S.M. (2015). Molecular underpinnings of prefrontal cortex development in rodents provide insights into the etiology of neurodevelopmental disorders. Mol. Psychiatry *20*, 795–809. https://doi.org/10.1038/mp.2014.147.

98. Bullmore, E.T., Frangou, S., and Murray, R.M. (1997). The dysplastic net hypothesis: an integration of developmental and dysconnectivity theories of schizophrenia. Schizophr. Res. *28*, 143–156. https://doi.org/10.1016/s0920-9964(97)00114-x.

99. Fatemi, S.H., and Folsom, T.D. (2009). The neurodevelopmental hypothesis of schizophrenia, revisited. Schizophr. Bull. *35*, 528–548. https://doi.org/10.1093/schbul/sbn187.

100. Horváth, S., and Mirnics, K. (2015). Schizophrenia as a disorder of molecular pathways. Biol. Psychiatry *77*, 22–28. https://doi.org/10.1016/j.biopsych.2014.01.001.

101. Chini, M., and Hanganu-Opatz, I.L. (2021). Prefrontal Cortex Development in Health and Disease: Lessons from Rodents and Humans. Trends Neurosci. *44*, 227–240. https://doi.org/10.1016/j.tins.2020.10.017.

102. Gao, R., Peterson, E.J., and Voytek, B. (2017). Inferring synaptic excitation/inhibition balance from field potentials. Neuroimage *158*, 70–78. https://doi.org/10.1016/j.neuroimage.2017.06.078.

103. Ramirez-Villegas, J.F., Besserve, M., Murayama, Y., Evrard, H.C., Oeltermann, A., and Logothetis, N.K. (2021). Coupling of hippocampal theta and ripples with pontogeniculooccipital waves. Nature *589*, 96–102. https://doi.org/10.1038/s41586-020-2914-4.

104. Adams, R.A., Bush, D., Zheng, F., Meyer, S.S., Kaplan, R., Orfanos, S., Marques, T.R., Howes, O.D., and Burgess, N. (2020). Impaired theta phase coupling underlies frontotemporal dysconnectivity in schizophrenia. Brain *143*, 1261–1277. https://doi.org/10.1093/brain/awaa035.

105. Lopes-Aguiar, C., Bueno-Junior, L.S., Ruggiero, R.N., Romcy-Pereira, R.N., and Leite, J.P. (2013). NMDA receptor blockade impairs the muscarinic conversion of sub-threshold transient depression into long-lasting LTD in the hippocampus-prefrontal cortex pathway in vivo: correlation with gamma oscillations. Neuropharmacology *65*, 143–155. https://doi.org/10.1016/j.neuropharm.2012.09.013.

106. Zavitsanou, K., Katsifis, A., Mattner, F., and Huang, X.F. (2004). Investigation of m1/m4 muscarinic receptors in the anterior cingulate cortex in schizophrenia, bipolar disorder, and major depression disorder. Neuropsychopharmacology *29*, 619–625. https://doi.org/10.1038/sj.npp.1300367.

107. Scarr, E., and Dean, B. (2009). Role of the cholinergic system in the pathology and treatment of schizophrenia. Expert Rev. Neurother. *9*, 73–86. https://doi.org/10.1586/14737175.9.1.73.

108. Dean, B., McLeod, M., Keriakous, D., McKenzie, J., and Scarr, E. (2002). Decreased muscarinic1 receptors in the dorsolateral prefrontal cortex of subjects with schizophrenia. Mol. Psychiatry *7*, 1083–1091. https://doi.org/10.1038/sj.mp.4001199.

109. Berman, J.A., Talmage, D.A., and Role, L.W. (2007). Cholinergic circuits and signaling in the pathophysiology of schizophrenia. Int. Rev. Neurobiol. *78*, 193–223. https://doi.org/10.1016/S0074-7742(06)78007-2.

110. Weinstein, J.J., Moeller, S.J., Perlman, G., Gil, R., Van Snellenberg, J.X., Wengler, K., Meng, J., Slifstein, M., and Abi-Dargham, A. (2024). Imaging the Vesicular Acetylcholine Transporter in Schizophrenia: A Positron Emission Tomography Study Using [(18)F]-VAT. Biol. Psychiatry *96*, 352–364. https://doi.org/10.1016/j.biopsych.2024.01.019.

111. Sun, Y., Rossi, A.M., Rahman, T., and Taylor, C.W. (2013). Activation of IP3 receptors requires an endogenous 1-8-14 calmodulin-binding motif. Biochem. J. *449*, 39–49. https://doi.org/10.1042/BJ20121034.

112. Ishii, M., and Kurachi, Y. (2006). Muscarinic acetylcholine receptors. Curr. Pharm. Des. *12*, 3573–3581. https://doi.org/10.2174/138161206778522056.

113. Bockaert, J., Perroy, J., Bécamel, C., Marin, P., and Fagni, L. (2010). GPCR interacting proteins (GIPs) in the nervous system: Roles in physiology and pathologies. Annu. Rev. Pharmacol. Toxicol. *50*, 89–109. https://doi.org/10.1146/annurev.pharmtox.010909.105705.

114. Ferré, S. (2015). The GPCR heterotetramer: challenging classical pharmacology. Trends Pharmacol. Sci. *36*, 145–152. https://doi.org/10.1016/j.tips.2015.01.002.

115. Koga, K., Matsuzaki, Y., Honda, K., Eto, F., Furukawa, T., Migita, K., Irie, K., Mishima, K., and Ueno, S. (2017). Activations of muscarinic M(1) receptors in the anterior cingulate cortex contribute to the antinociceptive effect via GABAergic transmission. Mol. Pain *13*, 1744806917692330. https://doi.org/10.1177/1744806917692330.

116. Zhong, P., Gu, Z., Wang, X., Jiang, H., Feng, J., and Yan, Z. (2003). Impaired modulation of GABAergic transmission by muscarinic receptors in a mouse transgenic model of Alzheimer's disease. J. Biol. Chem. *278*, 26888–26896. https://doi.org/10.1074/jbc.M302789200.

117. Xiao, Z., Deng, P.Y., Yang, C., and Lei, S. (2009). Modulation of GABAergic transmission by muscarinic receptors in the entorhinal cortex of juvenile rats. J. Neurophysiol. *102*, 659–669. https://doi.org/10.1152/jn.00226.2009.

118. Calcutt, N.A., Smith, D.R., Frizzi, K., Sabbir, M.G., Chowdhury, S.K.R., Mixcoatl-Zecuatl, T., Saleh, A., Muttalib, N., Van der Ploeg, R., Ochoa, J., et al. (2017). Selective antagonism of muscarinic receptors is neuroprotective in peripheral neuropathy. J. Clin. Invest. *127*, 608–622. https://doi.org/10.1172/JCI88321.

119. Kaul, I., Sawchak, S., Correll, C.U., Kakar, R., Breier, A., Zhu, H., Miller, A.C., Paul, S.M., and Brannan, S.K. (2024). Efficacy and safety of the muscarinic receptor agonist KarXT (xanomeline-trospium) in schizophrenia (EMERGENT-2) in the USA: results from a randomised, double-blind, placebo-controlled, flexible-dose phase 3 trial. Lancet *403*, 160–170. https://doi.org/10.1016/S0140-6736(23)02190-6.

120. Kranz, J., Petzinger, E., and Geyer, J. (2013). Brain penetration of the OAB drug trospium chloride is not increased in aged mice. World J. Urol. *31*, 219–224. https://doi.org/10.1007/s00345-011-0803-z.

121. Geyer, J., Gavrilova, O., and Schwantes, U. (2010). Differences in the Brain Penetration of the Anticholinergic Drugs Trospium Chloride and Oxybutynin. UroToday Int. J. *3*. https://doi.org/10.3834/uij.1944-5784.2010.02.12.

122. Barak, S., and Weiner, I. (2011). The M(1)/M(4) preferring agonist xanomeline reverses amphetamine-, MK801- and scopolamine-induced abnormalities of latent inhibition: putative efficacy against positive, negative and cognitive symptoms in schizophrenia. Int. J. Neuropsychopharmacol. *14*, 1233–1246. https://doi.org/10.1017/S1461145710001549.

123. Montani, C., Canella, C., Schwarz, A.J., Li, J., Gilmour, G., Galbusera, A., Wafford, K., Gutierrez-Barragan, D., McCarthy, A., Shaw, D., et al. (2021). The M1/M4 preferring muscarinic agonist xanomeline modulates functional connectivity and NMDAR antagonist-induced changes in the mouse brain. Neuropsychopharmacology *46*, 1194–1206. https://doi.org/10.1038/s41386-020-00916-0.

124. Anastasiades, P.G., and Carter, A.G. (2021). Circuit organization of the rodent medial prefrontal cortex. Trends Neurosci. *44*, 550–563. https://doi.org/10.1016/j.tins.2021.03.006.

125. Spencer-Smith, M., and Anderson, V. (2009). Healthy and abnormal development of the prefrontal cortex. Dev. Neurorehabil. *12*, 279–297. https://doi.org/10.3109/17518420903090701.

126. Wallis, J.D. (2007). Orbitofrontal cortex and its contribution to decision-making. Annu. Rev. Neurosci. *30*, 31–56. https://doi.org/10.1146/annurev.neuro.30.051606.094334.

127. Ghods-Sharifi, S., Haluk, D.M., and Floresco, S.B. (2008). Differential effects of inactivation of the orbitofrontal cortex on strategy set-shifting and reversal learning. Neurobiol. Learn. Mem. *89*, 567–573. https://doi.org/10.1016/j.nlm.2007.10.007.

128. Hasegawa, I., Hayashi, T., and Miyashita, Y. (1999). Memory retrieval under the control of the prefrontal cortex. Ann. Med. *31*, 380–387. https://doi.org/10.3109/07853899908998795.

129. Shin, J.D., and Jadhav, S.P. (2016). Multiple modes of hippocampal-prefrontal interactions in memory-guided behavior. Curr. Opin. Neurobiol. *40*, 161–169. https://doi.org/10.1016/j.conb.2016.07.015.

130. Sigurdsson, T., and Duvarci, S. (2015). Hippocampal-Prefrontal Interactions in Cognition, Behavior and Psychiatric Disease. Front. Syst. Neurosci. *9*, 190. https://doi.org/10.3389/fnsys.2015.00190.

131. He, Y., Wu, S., Chen, C., Fan, L., Li, K., Wang, G., Wang, H., and Zhou, Y. (2020). Organized Resting-state Functional Dysconnectivity of the Prefrontal Cortex in Patients with Schizophrenia. Neuroscience *446*, 14–27. https://doi.org/10.1016/j.neuroscience.2020.08.021.

132. Stark, K.L., Xu, B., Bagchi, A., Lai, W.S., Liu, H., Hsu, R., Wan, X., Pavlidis, P., Mills, A.A., Karayiorgou, M., et al. (2008). Altered brain microRNA biogenesis contributes to phenotypic deficits in a 22q11-deletion mouse model. Nat. Genet. *40*, 751–760. https://doi.org/10.1038/ng.138.

133. Carlén, M. (2017). What constitutes the prefrontal cortex? Science *358*, 478–482. https://doi.org/10.1126/science.aan8868.

134. Ährlund-Richter, S., Xuan, Y., van Lunteren, J.A., Kim, H., Ortiz, C., Pollak Dorocic, I., Meletis, K., and Carlén, M. (2019). A whole-brain atlas of monosynaptic input targeting four different cell types in the medial prefrontal cortex of the mouse. Nat. Neurosci. *22*, 657–668. https://doi.org/10.1038/s41593-019-0354-y.

135. Le Merre, P., Ährlund-Richter, S., and Carlén, M. (2021). The mouse prefrontal cortex: Unity in diversity. Neuron *109*, 1925–1944. https://doi.org/10.1016/j.neuron.2021.03.035.

136. Preuss, T.M., and Wise, S.P. (2022). Evolution of prefrontal cortex. Neuropsychopharmacology *47*, 3–19. https://doi.org/10.1038/s41386-021-01076-5.

137. Wong, S.K., Parker, E.M., and Ross, E.M. (1990). Chimeric muscarinic cholinergic: beta-adrenergic receptors that activate Gs in response to muscarinic agonists. J. Biol. Chem. *265*, 6219–6224. https://doi.org/10.1016/S0021-9258(19)39313-5.

138. Wess, J., Bonner, T.I., Dörje, F., and Brann, M.R. (1990). Delineation of muscarinic receptor domains conferring selectivity of coupling to guanine nucleotide-binding proteins and second messengers. Mol. Pharmacol. *38*, 517–523. https://doi.org/10.1016/S0026-895X(25)09481-7.

139. Wess, J., Blin, N., Mutschler, E., and Blüml, K. (1995). Muscarinic acetylcholine receptors: structural basis of ligand binding and G protein coupling. Life Sci. *56*, 915–922. https://doi.org/10.1016/0024-3205(95)00028-5.

140. Liu, J., Conklin, B.R., Blin, N., Yun, J., and Wess, J. (1995). Identification of a receptor/G-protein contact site critical for signaling specificity and G-protein activation. Proc. Natl. Acad. Sci. USA *92*, 11642–11646. https://doi.org/10.1073/pnas.92.25.11642.

141. Hu, J., Thor, D., Zhou, Y., Liu, T., Wang, Y., McMillin, S.M., Mistry, R., Challiss, R.A.J., Costanzi, S., and Wess, J. (2012). Structural aspects of M(3) muscarinic acetylcholine receptor dimer formation and activation. FASEB J. *26*, 604–616. https://doi.org/10.1096/fj.11-191510.

142. Högger, P., Shockley, M.S., Lameh, J., and Sadée, W. (1995). Activating and inactivating mutations in N- and C-terminal i3 loop junctions of muscarinic acetylcholine Hm1 receptors. J. Biol. Chem. *270*, 7405–7410. https://doi.org/10.1074/jbc.270.13.7405.

143. Blin, N., Yun, J., and Wess, J. (1995). Mapping of single amino acid residues required for selective activation of Gq/11 by the m3 muscarinic acetylcholine receptor. J. Biol. Chem. *270*, 17741–17748. https://doi.org/10.1074/jbc.270.30.17741.

144. Yohn, S.E., Weiden, P.J., Felder, C.C., and Stahl, S.M. (2022). Muscarinic acetylcholine receptors for psychotic disorders: bench-side to clinic. Trends Pharmacol. Sci. *43*, 1098–1112. https://doi.org/10.1016/j.tips.2022.09.006.

145. Paul, S.M., Yohn, S.E., Popiolek, M., Miller, A.C., and Felder, C.C. (2022). Muscarinic Acetylcholine Receptor Agonists as Novel Treatments for Schizophrenia. Am. J. Psychiatry *179*, 611–627. https://doi.org/10.1176/appi.ajp.21101083.

146. McCutcheon, R.A., Keefe, R.S.E., and McGuire, P.K. (2023). Cognitive impairment in schizophrenia: aetiology, pathophysiology, and treatment. Mol. Psychiatry *28*, 1902–1918. https://doi.org/10.1038/s41380-023-01949-9.

147. Veselinović, T., Vernaleken, I., Janouschek, H., Kellermann, T., Paulzen, M., Cumming, P., and Gründer, G. (2015). Effects of anticholinergic challenge on psychopathology and cognition in drug-free patients with schizophrenia and healthy volunteers. Psychopharmacology (Berl.) *232*, 1607–1617. https://doi.org/10.1007/s00213-014-3794-9.

148. Stanhope, K.J., Mirza, N.R., Bickerdike, M.J., Bright, J.L., Harrington, N.R., Hesselink, M.B., Kennett, G.A., Lightowler, S., Sheardown, M.J., Syed, R., et al. (2001). The muscarinic receptor agonist xanomeline has an antipsychotic-like profile in the rat. J. Pharmacol. Exp. Ther. *299*, 782–792. https://doi.org/10.1016/S0022-3565(24)29291-0.

149. Burger, W.A.C., Pham, V., Vuckovic, Z., Powers, A.S., Mobbs, J.I., Laloudakis, Y., Glukhova, A., Wootten, D., Tobin, A.B., Sexton, P.M., et al. (2023). Xanomeline displays concomitant orthosteric and allosteric binding modes at the M(4) mAChR. Nat. Commun. *14*, 5440. https://doi.org/10.1038/s41467-023-41199-5.

150. Fernández de Sevilla, D., Núñez, A., and Buño, W. (2021). Muscarinic Receptors, from Synaptic Plasticity to its Role in Network Activity. Neuroscience *456*, 60–70. https://doi.org/10.1016/j.neuroscience.2020.04.005.

151. Dickerson, D.D., Wolff, A.R., and Bilkey, D.K. (2010). Abnormal long-range neural synchrony in a maternal immune activation animal model of schizophrenia. J. Neurosci. *30*, 12424–12431. https://doi.org/10.1523/JNEUROSCI.3046-10.2010.

152. Sakurai, T., Gamo, N.J., Hikida, T., Kim, S.H., Murai, T., Tomoda, T., and Sawa, A. (2015). Converging models of schizophrenia–Network alterations of prefrontal cortex underlying cognitive impairments. Prog. Neurobiol. *134*, 178–201. https://doi.org/10.1016/j.pneurobio.2015.09.010.

153. Schizophrenia Working Group of the Psychiatric; Genomics Consortium (2014). Biological insights from 108 schizophrenia-associated genetic loci. Nature *511*, 421–427. https://doi.org/10.1038/nature13595.

154. Engmann, O., Labonté, B., Mitchell, A., Bashtrykov, P., Calipari, E.S., Rosenbluh, C., Loh, Y.E., Walker, D.M., Burek, D., Hamilton, P.J., et al. (2017). Cocaine-Induced Chromatin Modifications Associate With Increased Expression and Three-Dimensional Looping of Auts2. Biol. Psychiatry *82*, 794–805. https://doi.org/10.1016/j.biopsych.2017.04.013.

155. Andres-Alonso, M., Borgmeyer, M., Mirzapourdelavar, H., Lormann, J., Klein, K., Schweizer, M., Hoffmeister-Ullerich, S., Oelschlegel, A.M., Dityatev, A., and Kreutz, M.R. (2023). Golgi satellites are essential for polysialylation of NCAM and expression of LTP at distal synapses. Cell Rep. *42*, 112692. https://doi.org/10.1016/j.celrep.2023.112692.

156. Pennington, Z.T., Dong, Z., Feng, Y., Vetere, L.M., Page-Harley, L., Shuman, T., and Cai, D.J. (2019). ezTrack: An open-source video analysis pipeline for the investigation of animal behavior. Sci. Rep. *9*, 19979. https://doi.org/10.1038/s41598-019-56408-9.

157. Tian, R., Gachechiladze, M.A., Ludwig, C.H., Laurie, M.T., Hong, J.Y., Nathaniel, D., Prabhu, A.V., Fernandopulle, M.S., Patel, R., Abshari, M., et al. (2019). CRISPR Interference-Based Platform for Multimodal Genetic Screens in Human iPSC-Derived Neurons. Neuron *104*, 239–255.e12. https://doi.org/10.1016/j.neuron.2019.07.014.

158. Landgraf, P., Mikhaylova, M., Macharadze, T., Borutzki, C., Zenclussen, A.C., Wahle, P., and Kreutz, M.R. (2014). Binding of Y-P30 to syndecan 2/3 regulates the nuclear localization of CASK. PLoS One *9*, e85924. https://doi.org/10.1371/journal.pone.0085924.

159. Aravind, P., Chandra, K., Reddy, P.P., Jeromin, A., Chary, K.V., and Sharma, Y. (2008). Regulatory and structural EF-hand motifs of neuronal calcium sensor-1: Mg 2+ modulates Ca 2+ binding, Ca 2+ -induced conformational changes, and equilibrium unfolding transitions. J. Mol. Biol. *376*, 1100–1115. https://doi.org/10.1016/j.jmb.2007.12.033.

160. Bankhead, P., Loughrey, M.B., Fernández, J.A., Dombrowski, Y., McArt, D.G., Dunne, P.D., McQuaid, S., Gray, R.T., Murray, L.J., Coleman, H.G., et al. (2017). QuPath: Open source software for digital pathology image analysis. Sci. Rep. *7*, 16878. https://doi.org/10.1038/s41598-017-17204-5.

161. Schindelin, J., Arganda-Carreras, I., Frise, E., Kaynig, V., Longair, M., Pietzsch, T., Preibisch, S., Rueden, C., Saalfeld, S., Schmid, B., et al. (2012). Fiji: an open-source platform for biological-image analysis. Nat. Methods *9*, 676–682. https://doi.org/10.1038/nmeth.2019.

162. Grochowska, K.M., Gomes, G.M., Raman, R., Kaushik, R., Sosulina, L., Kaneko, H., Oelschlegel, A.M., Yuanxiang, P., Reyes-Resina, I., Bayraktar, G., et al. (2023). Jacob-induced transcriptional inactivation of CREB promotes Abeta-induced synapse loss in Alzheimer's disease. EMBO J. *42*, e112453. https://doi.org/10.15252/embj.2022112453.

163. Reddy, P.P., Raghuram, V., Hradsky, J., Spilker, C., Chakraborty, A., Sharma, Y., Mikhaylova, M., and Kreutz, M.R. (2014). Molecular dynamics of the neuronal EF-hand Ca2+-sensor Caldendrin. PLoS One *9*, e103186. https://doi.org/10.1371/journal.pone.0103186.

164. Catimel, B., Nerrie, M., Lee, F.T., Scott, A.M., Ritter, G., Welt, S., Old, L.J., Burgess, A.W., and Nice, E.C. (1997). Kinetic analysis of the interaction between the monoclonal antibody A33 and its colonic epithelial antigen by the use of an optical biosensor. A comparison of immobilisation strategies. J. Chromatogr. A *776*, 15–30. https://doi.org/10.1016/s0021-9673(97)00087-3.

165. Navarro, G., Aymerich, M.S., Marcellino, D., Cortés, A., Casadó, V., Mallol, J., Canela, E.I., Agnati, L., Woods, A.S., Fuxe, K., et al. (2009). Interactions between calmodulin, adenosine A2A, and dopamine D2 receptors. J. Biol. Chem. *284*, 28058–28068. https://doi.org/10.1074/jbc.M109.034231.

166. Wang, C., Ward, M.E., Chen, R., Liu, K., Tracy, T.E., Chen, X., Xie, M., Sohn, P.D., Ludwig, C., Meyer-Franke, A., et al. (2017). Scalable Production of iPSC-Derived Human Neurons to Identify Tau-Lowering Compounds by High-Content Screening. Stem Cell Rep. *9*, 1221–1233. https://doi.org/10.1016/j.stemcr.2017.08.019.

167. Fernandopulle, M.S., Prestil, R., Grunseich, C., Wang, C., Gan, L., and Ward, M.E. (2018). Transcription Factor-Mediated Differentiation of Human iPSCs into Neurons. Curr. Protoc. Cell Biol. *79*, e51. https://doi.org/10.1002/cpcb.51.

168. Karpova, A., Samer, S., Turacak, R., Yuanxiang, P., and Kreutz, M.R. (2023). Integration of nuclear Ca(2+) transients and subnuclear protein shuttling provides a novel mechanism for the regulation of CREB-dependent gene expression. Cell. Mol. Life Sci. *80*, 228. https://doi.org/10.1007/s00018-023-04876-8.

169. Karpova, A., Mikhaylova, M., Bera, S., Bär, J., Reddy, P.P., Behnisch, T., Rankovic, V., Spilker, C., Bethge, P., Sahin, J., et al. (2013). Encoding and transducing the synaptic or extrasynaptic origin of NMDA receptor signals to the nucleus. Cell *152*, 1119–1133. https://doi.org/10.1016/j.cell.2013.02.002.

170. Maximov, A., Pang, Z.P., Tervo, D.G.R., and Südhof, T.C. (2007). Monitoring synaptic transmission in primary neuronal cultures using local extracellular stimulation. J. Neurosci. Methods *161*, 75–87. https://doi.org/10.1016/j.jneumeth.2006.10.009.

171. Xia, Z., Arias-Gil, G., Deckert, M., Vollmer, M., Curran, A., Herrera-Molina, R., Brosch, M., Krug, K., Schmidt, B., Ohl, F.W., et al. (2019). Electrochemical Roughening and Carbon Nanotube Coating of Tetrodes for Chronic Single-Unit Recording. Preprint at bioRxiv. https://doi.org/10.1101/738245.

172. Onslow, A.C.E., Bogacz, R., and Jones, M.W. (2011). Quantifying phase-amplitude coupling in neuronal network oscillations. Prog. Biophys. Mol. Biol. *105*, 49–57. https://doi.org/10.1016/j.pbiomolbio.2010.09.007.

173. Rossant, C., Kadir, S.N., Goodman, D.F.M., Schulman, J., Hunter, M.L.D., Saleem, A.B., Grosmark, A., Belluscio, M., Denfield, G.H., Ecker, A.S., et al. (2016). Spike sorting for large, dense electrode arrays. Nat. Neurosci. *19*, 634–641. https://doi.org/10.1038/nn.4268.

174. Johnson, C., and Wilbrecht, L. (2011). Juvenile mice show greater flexibility in multiple choice reversal learning than adults. Dev. Cogn. Neurosci. *1*, 540–551. https://doi.org/10.1016/j.dcn.2011.05.008.

Please cite this article in press as: Oelschlegel et al., Elevated calneuron-1, an accessory subunit of muscarinic receptors, induces frontotemporal dysconnectivity and schizophrenia-like deficits, Neuron (2025), https://doi.org/10.1016/j.neuron.2025.10.038

STAR★METHODS

KEY RESOURCES TABLE

REAGENT or RESOURCE	SOURCE	IDENTIFIER
Antibodies		
Monoclonal mouse anti-GFP; Clone 6AT316.	Abcam	Cat: #ab38689; RRID: AB_732715
Polyclonal rabbit anti-GFP	Abcam	Cat: #ab6556; RRID: AB_305564
Monoclonal rat anti-HA (clone 3F10)	Roche	Cat: #11867423001; RRID: AB_390918
Polyclonal rabbit anti-tRFP	Evrogen	Cat: # AB233; RRID: AB_2571743
Polyclonal rabbit anti-CHRM1 (M1R)	Alomone Labs	Cat: #AMR-001; RRID: AB_2039993
Polyclonal rabbit anti-CHRM4	Alomone Labs	Cat: #AMR-004; RRID: AB_11219338
Polyclonal goat anti-CHRM1 (M1R)	Avantor/Everest Biotech	Cat: #EVBIEB07398; RRID:AB_10803673
Polyclonal guinea pig anti-MAP2	Synaptic Systems	Cat: #188004; RRID: AB_2138181
Polyclonal goat anti-mAChR M3, C-20	Santa Cruz	Cat: #sc-7474; RRID: AB_2260584
Polyclonal rabbit anti-calneuron-1	Produced in the lab	N/A
Polyclonal mouse anti-calneuron-1	Abnova	Cat: #H00083698-A01; RRID: AB_535135
Monoclonal mouse anti-MAP2, clone HM-2	Sigma-Aldrich	Cat: #PA1-10005; RRID: AB_1076848
Monoclonal mouse anti-MAP2-488, Alexa Fluor® 488 conjugated	Millipore	Cat: #MAB3418X; RRID: AB_571048
Polyclonal rabbit anti-Gαq11, C-19	Santa Cruz	Cat: #sc_392; RRID: AB_631537
Monoclonal mouse anti-β-actin	Sigma-Aldrich	Cat: #A2228; RRID: AB_476697
Normal rabbit IgG	Santa Cruz	Cat: #sc-2027; RRID: AB_737197
Chemicals, peptides, and recombinant proteins		
4′,6-Diamidino-2-phenylindole dihydrochloride (DAPI)	Sigma	Cat: #D9564
Mowiol 4-88 Reagent	Calbiochem/Merck Chemicals Ltd	Cat.: #475904
Gabazine (SR-95531)	Tocris	Cat.: #1262/10
Xanomeline	Merck	Cat.: #5058160001
Carbamoylcholine chloride	Sigma	Cat.: #C4382
Ipratropium bromide	Tocris	Cat.: #0692
Bicuculline	Tocris	Cat.: #0130/50
D-AP5	Tocris	Cat.: #0106/10
NBQX	Tocris	Cat.: #0373/10
Pirenzepine dihydrochloride	Tocris	Cat.: #1071/100
TTX	R&D Systems Tocris	Cat.: #1078/1; Cat.: #1069/1
Protease Inhibitor Cocktail	Roche	Cat.: #04693116001
PhosphoStop	Roche	Cat.: #04906837001
Duolink Proximity ligation assay	Sigma-Aldrich	Cat.: #DUO92101
Experimental models: Organisms/strains		
Mouse: C57BL/6J	The Jackson Laboratory	RRID: IMSR_JAX:000664
Mouse: B6-Caln1<em1Hhtg>/Hhtg	[155]	N/A
Mouse: Disc1Tm1Kara/+	[19]	N/A
Mouse: Df(16)A+/−	[132]	N/A
Oligonucleotides		
qPCR CALN1 human; F 5'- AAC TGT GTG GAG GCT GAG TG -3'	This paper	N/A
R 5'- CTT TGG GGA TCA AGG GGG TC -3'	This paper	N/A
qPCR GAPDH human; F 5'- TCA AGG CTG AGA ACG GGA AG -3'	This paper	N/A

(*Continued on next page*)

Please cite this article in press as: Oelschlegel et al., Elevated calneuron-1, an accessory subunit of muscarinic receptors, induces frontotemporal dysconnectivity and schizophrenia-like deficits, Neuron (2025), https://doi.org/10.1016/j.neuron.2025.10.038

Continued

REAGENT or RESOURCE	SOURCE	IDENTIFIER
R 5'- TCG CCC CAC TTG ATT TTG GA -3'	This paper	N/A
qPCR CALN1 mouse; F 5'-GCT ATC ATC ATG CAG CGT TT-3'	This paper	N/A
R 5'- AAG AAA ACC ATC CCG ACC TT -3'	This paper	N/A
qPCR GAPDH mouse; F 5'- ACC CAG AAG ACT GTG GAT GG -3'	This paper	N/A
R 5'- CAC ATT GGG GGT AGG AAC AC -3'	This paper	N/A
Sequencing primers Disc1 mouse; F 5′-TAGCCACTCTCATTGTCAGC-3′		N/A
R 5′-CCTCATCCCTTCCACTCAGC-3′		N/A
Sequencing primers Df16 mouse; F 5′-ATTCCCCATGGACTAATTATGGACAGG-3′		N/A
R 5′-GGTATCTCCATAAGACAGAATGCTATGC-3′		N/A
Software and algorithms		
Fiji/ImageJ	NIH	RRID: SCR_002285
GraphPad Prism 6	GraphPad Software	RRID: SCR_002798
R Studio	R Studio	RRID: SCR_000432
Igor Pro	Wavemetric	RRID: SCR_000325
Python	Python Software Foundation	RRID: SCR_008394
ANY-Maze	San Diego Instruments	RRID: SCR_014289
eZTrack	[156]	RRID: SCR_021496
MATLAB	MathWorks	RRID: SCR_001622
EEGLAB		RRID: SCR_007292
IMARIS	Oxford Instruments	RRID: SCR_007370
Minianalysis	Synaptosoft	RRID: SCR_002184
Clampex	Molecular Software	RRID: SCR_011323
Adobe Illustrator	Adobe	RRID: SCR_01027
1/f slope script	[102]	N/A
Spectral density ratio script	[103]	N/A
Bacterial and virus strains		
AAV9-hSyn-GFP	UKE Vector Facility	N/A
AAV9-hSyn-GFP-Caln-1	UKE Vector Facility	N/A
Biological samples		
Human brain samples	The Netherlands Brain Bank	N/A
Human brain samples	Navarrabiomed Biobank	N/A
Human brain samples	Galicia Sur Health Institute Biobank	N/A
Experimental models: Cell lines		
Monkey: COS7	ATCC	Cat: #CRL-1651; RRID: CVCL_0224
Human: HEK293T	ATCC	Cat: #CRL-3216 RRID: CVCL_0063
Human: i3-iPSCs	Dr. Ward by MTA[157]	N/A
Insect: SF9	Gibco	Cat: #11496015; RRID: CVCL_0549
Recombinant DNA		
pAAV-hSyn-GFP	This paper	N/A
pAAV-hSyn-GFP-calneuron-1	This paper	N/A
HA-M1R	Missouri S&T cDNA Resource Center	#MAR010TN00
pCMV-GFP-calneuron-1	This paper	N/A
pCMV-YFP-calneuron-1	This paper	N/A
pCMV-GFP-calneuron-1_Cterm	This paper	N/A

(*Continued on next page*)

Continued

REAGENT or RESOURCE	SOURCE	IDENTIFIER
pEGFP-C1	Clontech	Cat: V012024
Syndecan-2-myc	[158]	N/A
pCMV-GFP-calneuron-1_ΔTMD	[71]	N/A
pCMV-GFP-calneuron-1- ΔEF1/2	This paper	N/A
GST-M1R-I3	Missouri S&T cDNA Resource Center	#MAR0100000
Caldendrin	[71]	N/A
Calmodulin	This paper	N/A
NCS-1	[159]	N/A
His6SUMO-calneuron-1_ ΔTMD	[71]	N/A
pCMV-Gαq11-YFP	This paper	N/A
pCMV-M1R-TagRFP	This paper	N/A
shRNA_calneuron-1; 5'-CAGTTGGCTAATATCTCTG-3'	GeneCopoeia	Cat.: #RSH048681

EXPERIMENTAL MODEL AND SUBJECT DETAILS

Animals

All animal experimental procedures were approved by the responsible authorities of Saxony-Anhalt (SA, Landesverwaltungsamt für Verbraucherschutz und Veterinärangelegenheiten, Referat 203) and Hamburg (HH; Behörde für Justiz und Verbraucherschutz, Amt für Verbraucherschutz, Lebensmittelsicherheit und Veterinärwesen). **SA**: RNAscope experiments were carried out on heterozygous genetically engineered mutant Disc1 mice carrying a Disc1 allele (Disc1Tm1Kara) on a C57BL/6J background.[19] As a second model, the Df(16)A+/− model (here Df16) was used.[132] For patch-clamp recordings from calneuron-1 deficient mice, male and female *CALN1*-KO mice (B6-Caln1<em1Hhtg, on a C57BL/6J background) or non-transgenic littermates were used at 13-15 weeks of age. All other electrophysiological recordings and patch-clamp analyses, all electrophysiological experiments in freely moving animals and the behavior experiments for PPI, LI, OF/NOR/NOL were obtained from or conducted with male C57BL/6J mice injected with AAV expressing either GFP-Caln-1 or GFP under control of human synapsin promoter. Mice were between 8 and 11 weeks old at the time of injection. All mice were group housed on a 12 h light / 12 h dark cycle until either two days before tetrode implantation or until habituation for behavioral experiments started. Food and water were available *ad libitum*. **HH**: Electrophysiological and/or behavioral experiments were conducted on group housed C57BL/6J mice, ranging from postnatal day (P) 5 to P75, of both sexes. Pregnant dams were individually housed, and weaned offspring were housed with at least two cage-mates on a 12 h light / 12 h dark cycle. Where not indicated otherwise, food and water were available *ad libitum*. The day of vaginal plug detection was considered embryonic day (E) 0.5, while the day of birth was considered P0. All mice that underwent electrophysiological investigations *in vivo* were also tested in the discrimination and reversal task as well as for their working memory abilities. Additionally, a separate group of mice was used exclusively for behavioral investigations of set-shifting and object recognition abilities.

Human brain samples

Human brain samples and data from patients included in this study were provided by the Netherlands Brain Bank (www.brainbank.nl), the Navarrabiomed Biobank and the Biobank at the Galicia Sur Health Research Institute and they were processed following standard operating procedures with the appropriate approval of the Ethics and Scientific Committees, specifically the local ethics committee in Magdeburg (Reference number 17/24). Further information on the human subjects can be found in the Table S1.

METHOD DETAILS

Quantitative real-time PCR

RNA was isolated from human and mouse brain samples using the RNeasy Plus Micro Kit and RNeasy Plus Mini Kit, respectively (Qiagen, Valencia, CA, USA). Briefly, 50 ng of RNA were reverse transcribed using random nonamers (Sigma-Aldrich, St. Louis, MO, USA) following the manufacturer's instructions (Sensiscript, Qiagen). Both mRNA species, *CALN1* and *glyceraldehyde 3-phosphate dehydrogenase* (GAPDH) as the reference gene, were amplified using the iScript RT-PCR iQ SYBR Green Supermix (Bio-Rad, Hercules, CA, USA) within a real-time quantitative PCR (qPCR) detection system (LC480, Roche, Basel, Switzerland). Details for primer sequences that were used can be found in the key resources table. The relative expression levels were analyzed using the $2^{-\Delta\Delta ct}$ method, with normalization relative to the housekeeping gene. Significant differences (*p<0.05, **p<0.01 and ***p<0.001) between the groups were calculated using one-tailed t-test for the human data and 1-way ANOVA for the mouse models of schizophrenia.

Please cite this article in press as: Oelschlegel et al., Elevated calneuron-1, an accessory subunit of muscarinic receptors, induces frontotemporal dysconnectivity and schizophrenia-like deficits, Neuron (2025), https://doi.org/10.1016/j.neuron.2025.10.038

RNAscope

Fresh-frozen brain sections from WT, Disc1 and Df16 animals were sectioned at a thickness of 16 μm and stored at -80°C overnight. Slices were fixed in 4% paraformaldehyde at 4°C for 1 hour, subsequently dehydrated by 5-minute baths with increasing alcohol concentrations (50%, 70%, 100%, 100%) and air-dried for 10 minutes before being treated with hydrogen peroxide for 10 minutes at RT and washed two times with water. Following this, slices were incubated with protease IV for 20 minutes at RT and washed two times with PBS. The sections were then hybridized with the *CALN1* transcript variant 1 mRNA probe at 40°C for 2h in a HybEZ™ oven (ACD). The slices were then washed two times using the Wash buffer. The signal was next amplified using the RNAscope® Multiplex Fluorescent Detection Reagents v2 and the signal was detected using TSA Vivid™ fluorophore 520 at a 1/1500 dilution. Finally, the sections were counterstained with DAPI and mounted with ProLong™ Gold. Slides were imaged at 20X and the number of puncta per cells was quantified using the QuPath software.[160] Statistical differences (*p<0.05, **p<0.01, ****p<0.0001) between groups on nested data were analyzed with linear mixed-effect models. Parameter estimation was done using the *lmer* function implemented in the *lme4* R package. To test the significance of condition (group) in the model, a likelihood ratio test against a reduced model was performed in which condition was removed (*lmerTest* R package). The full model included the following parameters: Measured parameters ~ condition + (1 | animal). For multiple group comparisons of the mouse models of schizophrenia against the WT animals, post hoc analysis with Holm's multiple comparison correction was carried out using the *contrasts* function of the *emmeans* R package.

Quantitative immunoblot analysis of human brain tissue

Human brain tissue was homogenized in the homogenization buffer containing 5 mM HEPES and 320 mM sucrose (pH 7.4), supplemented with the Protease Inhibitor Cocktail and PhosphoStop, and the resulting pellet was resuspended using 2×Laemmli buffer. A TRIzol-based extraction procedure was applied to mouse brain homogenates. Equal amounts of protein were loaded on 4–20% gradient polyacrylamide gels and subsequently transferred onto polyvinylidene difluoride (PVDF) membranes. For protein detection, membranes were incubated with anti-calneuron-1 and beta-actin (Sigma-Aldrich) antibodies. Integrated density values were assessed for the analysis using Fiji[161] and normalized to control samples. Significant differences (*p<0.05 and **p<0.01) between the groups were calculated using one-tailed t-test.

Protein extraction from transfected HEK293T cells and immunoprecipitation

For heterologous co-immunoprecipitation (Co-IP) HEK293T cells were transfected with different combinations of EGFP-, HA-, -tagged constructs using calcium phosphate method as described before, see for example.[162]

Expression and purification of bacterially produced recombinant proteins

All recombinant bacterial proteins were purified from *E. coli* BL21 (DE3). Purification protocols followed published procedures.[71,163] GST-tagged proteins were purified on Glutathione Sepharose 4B as well as on Protino® Glutathione Agarose 4B using Tris-buffered saline (TBS, pH 7.6) as purification buffer. Purification of GST-tagged proteins was carried out either in batch format or in self-packed columns using gravity flow. His_6SUMO-fusion proteins were purified on ProBond resin same way as GST-tagged proteins or preferential on 1 ml HisTrap HP columns using a ÄKTApurifier10 FPLC-system (GE Healthcare). Myriostylated NCS-1 was purified on phenyl-Sepharose fast flow matrix (Pharmacia) as described previously.[72]

Pull-down experiments

Pull down experiments with immobilized GST-M1R_I3 protein or GST as control were carried out using 6xHis-tag purified calneuron-1_ΔTMD and/or G protein alpha q. In brief, after determination of the concentration GST-proteins bound to Protino® Glutathione Agarose 4B, 3 μg were incubated with 0.5-1 μg of calneuron-1_ΔTMD and $G\alpha q_{11}$ extracted from SF9 cells in TBS for 1 hour at RT in the presence of 500 μM Ca^{2+} or 1 mM EGTA. After removal of unbound and extensive washing, proteins were eluted from the beads using 2xSDS sample buffer and finally subjected to immunoblotting.

Surface plasmon resonance

Surface plasmon resonance (SPR) binding studies of GST-M1R-I3 loop or GST control to 6xHis-SUMO-calneuron-1_ΔTMD, untagged Caldendrin, untagged myristoylated NCS-1 and untagged CaM were performed on a Biacore X100 instrument equipped with the sensor chip CM5 (GE Healthcare) at 25°C. GST-M1R-I3 loop / GST were coupled to the sensor chip cell according to the manufacturer's instructions. After equilibrating the sensor chip with HBS-P (10 mM HEPES pH 7.4, 150 mM NaCl and 0.005% Surfactant P20) at a flow rate of 10 μl/min, the chip surface was activated with a 7-minute pulse of 50 mM N-hydroxysuccinimide / 200 mM N-ethyl-N'-(dimethylaminopropyl)-carbodiimide at a flow rate of 10 μl/min. Subsequently the GST-M1R-I3 loop was immobilized on the surface of the sensor chip cell by injecting a 7-minute pulse of ligand solution (20 μg/ml of GST-M1R-I3 loop in 10 mM sodium acetate pH 4.5). Excess of reactive groups on the chip surface was deactivated with a 7-minute pulse of 1M ethanolamine hydrochloride pH 8.5, at a flow rate of 10 μl/min. Binding studies with calcium sensor proteins were done either in the presence (10 mM HEPES pH 7.4, 150 mM NaCl, 200μM Ca^{2+}, 500μM Mg^{2+} and 0.005% Surfactant P20) or the absence of Ca^{2+} (10 mM HEPES pH 7.4, 150 mM NaCl, 200μM EGTA, 1mM Mg^{2+} and 0.005% Surfactant P20). Each run was performed at a 10 μl/min flow rate and 1 min equilibration of the chip with the indicated analysis buffer. Afterwards the analyte was injected in a 3-min pulse

(association time) followed by a 3-min pulse with analysis buffer alone (dissociation time). Single cycle mode titrations and individual runs were finished with the regeneration of the chip matrix using a 2-min pulse of regeneration buffer (0.1M glycine pH 2.0) at a flow rate of 10 μl/min. The molar binding activity (MBA) was calculated from the stability point of each injection and determined as the molecular mass of both interacting partners in relation to the amount of GST-M1R-I3 immobilized on the sensor surface.[164]

Cell culture and transfection

Culture conditions and transfection of HEK293T and COS7 cells were described previously.[71] SF9 cells were maintained according to the manufacturer's guidelines (Gibco). Primary neurons were kept in Neurobasal medium (NB/GIBCO/Life Technologies) supplemented with B27 (GIBCO/Life Technologies), L-Glutamine (GIBCO/Life Technologies) and penicillin / streptomycin (PAA Laboratories, Pasching, Austria). Neurons were transfected at DIV13 with shRNA plasmids or at DIV16 with cDNA plasmids using Lipofectamine 2000 (Invitrogen). After transfection neurons were kept for additional 48 (cDNA plasmids) or 96 hours (shRNA plasmids) before recording. For immunocytochemistry experiments neurons were transfected at DIV12/13 and fixed 48 hours later.

FRET assay

In vivo FRET assays were conducted following the protocol described previously.[165] The cell suspension was then analyzed using a Fluostar Optima Fluorimeter (BMG Labtechnologies). Significant differences (*p<0.05, **p<0.01 and ***p<0.001) between the groups were calculated using either one-tail Student's t-test or 2-way ANOVA, where post hoc analysis was done with Bonferroni's tests.

Human i3-iPSCs derived neurons

As a source of human neurons for investigating the association between calneuron-1 with M1R through proximity ligation, we utilized the constitutive CRISPRi-Ngn2-WTC11, a stable transgenic line of human iPSCs. This line features a doxycycline inducible Ngn2 transcription factor and was obtained via the MTA (2021-0337) from Dr. M.E. Ward, (NINDS, NIH, HHS;[157]). To differentiate human iPSCs into i3Neurons (integrated, inducible, and isogenic), we employed a simplified two-step protocol as previously described.[166,167] Initially, i3N-iPSCs were thawed and plated onto Matrigel-coated six-well plates in doxycycline-supplemented (2 μg/ml) knockout Dulbecco's modified Eagle's medium (KO-DMEM)/F12 medium for 3 days to initiate pre-differentiation.[166] The pre-differentiated i3N precursor cells were subsequently dissociated and subplated onto poly-l-ornithine-(PLO)-coated 18mm coverslips at the 100.000 cell/well in 12-well plates. Maturation medium, supplemented with conditioned NB (Gibco) medium from rat glial cultures, was used, and i3Neurons were maintained until DIV61.

Immunocytochemistry, immunohistochemistry and proximity ligation assay

Immunocytochemical and immunohistochemical analysis were performed as described before, see for example.[162] The following commercial primary antibodies were used in the current study: anti-GFP (Abcam), anti-M1R (Alomone Labs), anti-M1R (Avantor), anti-calneuron-1 (Abnova), anti-calneuron-1 (Novus), anti-MAP2-488, Alexa Fluor® 488 conjugated (Millipore). Average or maximal intensity values were assessed for the analysis using FiJi (https://fiji.sc) and normalized to control samples. For the proximity ligation, i3Neurons and brain sections underwent washing with Duolink wash buffer A (Sigma-Aldrich) followed by an incubation with Duolink PLA probes PLUS and MINUS either in a humidity chamber or in 48 well plate respectively, both for 1 h at 37°C. Subsequently, coverslips and slices were washed with buffer A and incubated with ligase for 1 hour at 37°C. For amplification step, coverslips and slices were incubated with polymerase and Duolink FarRed Detection Reagent at 37°C for 100 minutes. After completing the washing stages, i3Neurons were treated with anti-MAP2 antibodies conjugated to Alexa Fluor488® and subsequently mounted using Mowiol 4–88. Significant differences (***p<0.001) between the groups were calculated using either one-tailed Student's t-test or 1-way ANOVA, where post hoc analysis was done with Bonferroni's tests.

Confocal Laser Scanning Microscopy and Image Analysis

Confocal laser scanning microscopy and Image Analysis were done as described previously.[168,169]

Viral constructs and viral particle production

The open reading frames (ORFs) for GFP and GFP-Caln-1 were subcloned into the AAV-hSyn vector using EcoRI/HindIII restriction sites. AAV particles expressing either GFP or GFP-calneuron-1 were produced at the UKE Vector Facility, Hamburg as an AAV9 serotype.

Lentiviral knockdown of calneuron-1 in rat striatal primary cultures

Lentiviral particles for the knockdown of calneuron-1 were produced in HEK293T-cells. The desired scrambled control sequence containing vector or the pLL3.7-shLuc and pLKO.1-415 with the psPAX2 and the pCMV-VSV-G vector were used for packaging in a ratio of 4:2:1. Triple-transfections were carried out using the calcium phosphate method with 20 μg total DNA/T75 flask directly after media exchange to fresh DMEM + (containing FCS, glutamine and pen/strep). 6-8 hours after application of the transfection mix, medium was completely exchanged to NB+. Culture supernatant was collected 48 hours after transfection, clarified and sterile filtered using a 0.45 μm syringe filter. Remaining supernatant was aliquoted and immediately frozen at -80°C. Infections with a Lentivirus carrying the calneuron-1 shRNA or scrambled control were performed on DIV2 striatal primary neurons seeded in 6-well plates.

About 1h prior to infection, half of the culture media was collected from each well and replaced by NB+ media. The collected conditioned media was then diluted by adding the equal volume of NB+ and kept overnight at 4°C. For the infection 600 μl (equals 30% media volume) of virus-containing HEK293T-cell supernatant were added per well. About 24 h after infection the media was replaced by conditioned media and cells were kept for another 4 days in incubator. The knockdown efficiency was analyzed by immunoblotting with calneuron-1 specific antibody and normalized to scrambled control. Significant differences (***p<0.001 and ****p<0.0001) between the groups were calculated using 1-way ANOVA; post hoc analysis was done with Tukey's multiple comparison.

mPFC slice preparation and fEPSP recording

Coronal slices containing the prelimbic PFC from mice injected with AAV expressing either GFP-calneuron-1 or GFP under control of a human synapsin promoter, were prepared and paired-pulse field excitatory postsynaptic potentials (fEPSPs) were recorded following the protocol described by Ghoshal et al.[60] The stimulation was applied to the superficial layers II-III using a concentric bipolar stimulation electrode. The fEPSPs were recorded using capillary microelectrodes filled with ACSF (3-5 MΩ) and amplified by an Extracellular Amplifier (EXT-02B, npi, Germany). The recorded signals were digitized at a sampling frequency of 5 kHz using a Digidata 1401plus AD/DA converter (CED, England) and lowpass filtered. Robust short-term depression followed by moderate muscarinic LTD (mLTD) was induced by bath-application of 50 μM carbachol (Cch) for 10 minutes. The Cch-induced LTD in the mPFC was recorded for 60 minutes following the application of Cch. The data are presented as the mean ± SEM. Statistical differences (*p<0.05 and **p<0.01) between groups on nested data were analyzed with linear mixed-effect models. Parameter estimation was done using the *lmer* function implemented in the *lme4* R package. To test the significance of condition (group) in the model, a likelihood ratio test against a reduced model was performed in which condition was removed (*lmerTest* R package). The full model included the following parameters: Measured parameters ~ condition + (1 | animal). For multiple group comparisons of Xanomeline treated mice, post hoc analysis with Holm's multiple comparison correction was carried out using the *glht* function of the *multcomp* R package.

Miniature inhibitory postsynaptic current (mIPSC) recordings in coronal brain slices and striatal primary neurons

Coronal brain slices (300 μm) were produced using sucrose solution following composition (in mM): 60 NaCl, 100 sucrose, 2.5 KCl, 1.25 NaH_2PO_4, 26 NaHCO3, 1 $CaCl_2$, 5 $MgCl_2$, 20 glucose, oxygenated with 95% O_2 and 5% CO_2). After cutting, slices were incubated for 30 minutes in the water bath at 34°C before being transferred to the recording solution ACSF with the following composition (in mM): 125 NaCl, 3 KCl, 1.25 $NaH2PO_4$, 26 $NaHCO_3$, 2.6 $CaCl_2$, 1.3 $MgCl_2$, 15 glucose, oxygenated with 95% O_2 and 5% CO_2. Voltage-clamp whole cell patch-clamp recordings were performed in the prefrontal cortex (L2/3) and visualized with an Olympus microscope (BX51WI). The signals were acquired with ELC-03XS (npi) amplifiers at 50 kHz via LIH 8+8 interface (HEKA) and Igor Pro 8 software (WaveMetrics). The recording pipettes with a resistance of 4–6 MΩ were filled with intracellular solution containing (in mM): 140 Cs-Gluconate, 7 CsCl, 5 HEPES-acid, 0.16 EGTA, 0.5 $MgCl_2$, 5 Phosphocreatine (pH 7.3 with CsOH, 289 mOsm), and implemented with biocytin. Cell capacitance was canceled; series resistance was compensated and did not exceed 35 MΩ. Neurons were recorded at a holding potential of 0 mV without correction of the liquid junction potential.

For mIPSC measurements, glutamatergic synaptic transmission was blocked with NBQX (10 μM) and D-AP5 (50 μM). In addition, TTX (1 μM) was bath applied to prevent firing of the neurons. In several experiments Gabazine (SR-95531, 10 μM) was added to the bath solution to demonstrate the GABAa-dependence of the mIPSCs. Only neurons with recording time exceeding 5 minutes were included into the analysis. All mIPSC events that exceeded the onset threshold, which is 5 pA higher than the standard deviation of the recordings filtered with highpass filter (6Hz), were detected with custom-made python script. The median frequency and median amplitude of mIPSC events within the animals were calculated. Significant differences (*p<0.05 and **p<0.01) between the groups were calculated using Mann-Whitney U-test.

For analysis of frequency and amplitude in the presence of xanomeline, xanomeline-oxalate (10mM) was washed in for 10 minutes via perfusion after a five-minute baseline period. The five minutes of baseline and the last five minutes after xanomeline was washed in were used for analysis. To evaluate the effects of genotype and experimental condition on slopes, a linear mixed-effects (LME) model was employed using the statsmodels package in Python. The model included *genotype (WT/KO)*, *condition (with/without Xanomeline)*, and their interaction (*genotype* × *condition*) as fixed effects, and *mouse ID* as a random effect to account for repeated measures within subjects.

mIPSCs of striatal primary neurons (DIV15-21) were recorded under whole-cell voltage clamp conditions using 3-5 MΩ pipettes filled with an 'intracellular' solution containing (in mM): 135 CsCl, 1 EGTA, 10 HEPES, 4 ATP-Mg_2, 1 GTP-Na_2, pH 7.4 with CsOH (290 mOsm).[170] To block spontaneous action potential generation 0.5 μM TTX was added to the extracellular solution that contained (in mM): 140 NaCl, 5 KCl, 2 $CaCl_2$, 0.8 $MgCl_2$, 10 HEPES, 10 glucose, pH 7.40 with NaOH (285 mOsm). Neurons plated on coverslips were transferred to a RC26 GLP recording chamber (Warner Instruments) mounted on a Leica SP2 microscope equipped with 40x water dipping objective and were constantly perfused with extracellular solution at a rate of 1 ml/min at room temperature (25°C). mIPSCs were recorded with an Axopatch 200B (Molecular Devices) amplifier and digitalized with Digidata 1440 and acquired by Clampex 10 software (Molecular Devices). Membrane potential was held at -60 mV and current traces were filtered at 2 kHz lowpass basal filter and digitized at 10 kHz. Continuous recording of current traces was followed by off-line analysis of using Minianalysis 6 software (Synaptosoft). Only whole cell voltage-clamp recordings from cells with a membrane resistance of 100 to 300 MΩ and a holding current of less than 200 pA were included in the analysis. The temperature in the recording chamber (25°C) was controlled by a TC344B dual temperature controller (Warner Instruments). Absolute values from control conditions were taken as 100% ± SEM.

Significant differences (*p<0.05) between the groups were calculated using 2-way ANOVA, where post hoc analysis was done with Bonferroni's tests.

In vivo recordings in mice overexpressing calneuron-1 developmentally

Intracortical AAV injections in pups

At P5, pups were injected bilaterally with 120 nl of AAV particles expressing either GFP or GFP-calneuron-1 into the mPFC (0.5 mm anterior to bregma, 0.1-0.5 mm lateral to the midline, 1.6 mm deep). The first recordings were not performed earlier than 25 days after injection, to enable reliable viral expression. Each litter of mice was divided into Caln-1 (GFP-Caln-1) and control (GFP) mice to reduce litter-dependent variability.

Adapter implantation for head-fixed recordings

The adapter for head fixation was implanted at least 5 days before electrophysiological recordings. A metal head-post (Neurotar, Helsinki, Finland) was attached to the exposed and cleaned skull with dental cement, and a craniotomy was performed above the mPFC (0.5-2.0 mm anterior to bregma, 0.1-0.5 mm right to the midline) and intermediate HP (iHP; 1-1.5 mm anterior to lambda, 4.5-5.0 mm right to the midline), protected by a custom synthetic window filled with Kwik-Cast sealant (World Precision Instruments, Friedberg, Germany). A silver wire (AG-8W, Science Products) was implanted between the skull and brain tissue above the cerebellum, served as ground and reference.

Head-fixed chronic recordings calneuron-1 overexpression during development

Simultaneous multisite extracellular recordings were performed unilaterally in the right hemisphere of the mPFC and iHP of P30-32 GFP-calneuron-1 and GFP-control mice. After recovery from the surgery, mice were accustomed to head-fixation and trained to move in the Mobile HomeCage recording system (Neurotar, Helsinki, Finland). For recordings, craniotomies were uncovered and multi-site electrodes (NeuroNexus, MI, USA) were stereotactically inserted into the mPFC (four-shank, A4x8 recording sites, 50 μm spacing, 1.6 mm deep, covering all prefrontal layers) and iHP (one-shank, A1x16 recording sites, 50 μm spacing, 1.6 mm deep, crossing the *stratum pyramidale*). Extracellular signals were band-pass filtered (0.1-9000 Hz) and digitized (32 kHz) with a multichannel extracellular amplifier (Digital Lynx SX; Neuralynx, Bozeman, MO, USA). Recordings were acquired for 45 min to 1 h. After recordings, the craniotomy was closed, and mice were returned to their home cage. The same animals were recorded up to 2 times. Electrode position was confirmed in brain slices postmortem. For LFP analysis of prefrontal activity, a recording channel within the mPFC and for LFP analysis of hippocampal activity a recording channel within the *stratum pyramidale* close to the electrical reversal was selected.

Verification of construct expression and electrode position

After completing electrophysiological recordings and behavioral tests, the animals underwent transcardial perfusion using a 4% PFA solution in 1xPBS. Following perfusion, the brains were postfixed in 4% PFA for 24 hours at 4°C and subsequently transferred into a 30% sucrose solution. Coronal brain sections with a thickness of 40 μm were obtained using a microtome (Leica, Germany, CM3050 S), and expression of the transgene was analyzed by confocal microscopy. For mice that underwent electrophysiological recordings, brains were sectioned coronally at 100 μm for post-mortem electrode reconstruction. To maintain consistency in data analysis, animals displaying asymmetrical expression - those lacking expression in both hemispheres or showing negligible expression in one hemisphere - were systematically excluded from the study.

In vivo recordings in mice overexpressing calneuron-1 in adulthood

Intracortical AAV injections

For overexpression of either GFP-calneuron-1 or GFP, mice (male, single housed, 8-10 weeks old) were injected with 600 nl virus of AAV-hSyn-GFP-calneuron-1 ($1x10^{13}$; GFP-calneuron-1 mice) or AAV-hSyn-GFP ($5x10^{12}$; GFP-control mice) bilaterally into the medial prefrontal cortex (mPFC) (1.8 mm AP & +/- 0.3 mm L/R from Bregma as well as 2.2 mm DV from skull).

Mice that were intended for chronic electrophysiological recordings were injected at 8 weeks of age, coordinates for viral injection were slightly modified (1.78 mm AP & +/- 0.3 mm L/R from Bregma as well as 1.63 mm DV from brain surface).

Electrode implantation in adult mice

Surgery was performed 18-20 days post viral injection. One carbon nanotube coated tetrode each was implanted bilaterally into the mPFC (1.78 mm AP & +/- 0.3 mm L/R from Bregma as well as 1.66 mm DV from brain surface) and the anterior dorsal hippocampus (dHP; -2.7 mm AP & +/- 2.75 mm L/R from Bregma as well as 1.25 mm DV from brain surface). Six burr holes were drilled into the skull, two right and left over the PFC for reference electrodes (AG-3T, Science products; chlorided just prior to surgery and implanted subcranially), two right and left over the PFC for virus injection and tetrode implantation (.001 PLATINUM 20% IRIDIUM Heavy Teflon coating, Stress Relieved temper, California Fine Wire Company; carbon nanotube coated) and two over the hippocampus (HP) for tetrode implantation. Tetrode implantation was done under control of acute intra-surgical recordings (Intan Technologies). Two screws (countersunk 1 x 3 mm) were added to stabilize the head plug later on and for fixation of grounds (AG-8W, Science Products). In addition, two muscle wires (7SS-1T, Science products) were implanted into the neck of each animal. All wires were prefixed onto a custom made laterally oriented circuit board plug[171] and fixed in position with UV glue before the circuit board and surplus wire was fixed to the skull with dental cement in a way to result in a stable head plug, altogether not exceeding a weight of 1.2 mg; the skin was attached evenly to it.

Please cite this article in press as: Oelschlegel et al., Elevated calneuron-1, an accessory subunit of muscarinic receptors, induces frontotemporal dysconnectivity and schizophrenia-like deficits, Neuron (2025), https://doi.org/10.1016/j.neuron.2025.10.038

Xanomeline-trospium (XT) treatment

Treatment of XT started two days before behavioral assessment or electrophysiological recordings. XT was applied once a day with trospium-chloride (4mg/kg body weight; stock preparation: 0.5mg in 200µl H_2O & 100µl MediGel Sucralose; trospium dose was increase from 1 to 4 mg/kg body weight over the first two batches of mice to alleviate remaining signs of nausea) being force fed two hours before the subcutaneous injection of xanomeline-tartrate (10mg/kg body weight; in 0.9% sodium-chloride), itself 30 minutes prior to behavioral assessment or onset of recordings. Assessment of locomotor activity was performed 1 hour after xanomeline injection, after mice had regained locomotor activity in their home cage. Both stock solutions were refrigerated after stock preparation to be used within six days.

Chronic recordings after calneuron-1 overexpression in adult mice

Simultaneous multisite extracellular recordings were performed bilaterally in the left and right hemisphere of the mPFC and the anterior dorsal hippocampus. Extracellular signals were recorded and digitized (30 kHz) using an Intan RHD 32-channel headstage and an Intan RHD 2000 USB interface board (Intan Technologies). Recordings were acquired in two mice simultaneously (one treated with vehicle, the other with XT) for 1 hour during the day with lights on in a soundproof chamber. For this, mice remained to freely roam in their home cage. To prevent climbing out, cages were each surrounded by a higher walled box that was open to the top and had two transparent and two nontransparent walls. Recordings from the same animals were repeated daily 30 minutes after xanomeline or vehicle injection for five consecutive days. Electrode position was confirmed in brain slices post mortem.

Lesioning, perfusion, and brain slicing

To validate virus expression and proper tetrode position, mice were subjected to a lesioning protocol after all experiments were concluded and prior to transcardial perfusion. For this, mice were deeply anaesthetized by intraperitoneal ketamine/xylazine injection and placed onto a heating pad; the head plug was connected to a multichannel lesion plug, which was connected to a pulse stimulator, and 20µA current was applied to each tetrode individually for 10 seconds. Afterwards, the mice were kept unconscious for 1 hour to allow lesions to form at the tip of the tetrodes. Boosters of anesthesia were given if or when reflexes returned – before they were perfused transcardially with 0.9% saline and 4% paraformaldehyde (Histofix, Carl Roth, Germany). Brains were removed, post-fixed in 4% paraformaldehyde for 24 h, transferred to 0.5 & 1 M sucrose and stored at -80°C before being sectioned coronally with a vibratome at 30 µm for sections of the PFC and 40 µm for sections of the HP. Recordings were considered from mice where virus expression matched tetrode position and tetrode position was located within the medial PFC and the dorsal HP. Lesion size did not allow for layer specific validation of location.

Analysis of electrophysiological data

LFP analysis – developmental overexpression

In vivo data were analyzed with custom-written algorithms in MATLAB environment. Ninety randomly selected, noise-free, 10 s-long signal segments were extracted from recordings with a typical duration of 45 min to 1 h and band-pass filtered (0.5-100 Hz) using a third-order Butterworth filter forward and backward to preserve phase information before down-sampling to a sampling rate of 200 before analyzing the LFP.

LFP analysis – overexpression during adulthood

In vivo data were analyzed with custom-written algorithms in MATLAB environment. Thirty randomly selected, noise-free, 10 s-long signal segments were extracted from the first five minutes of recording and 30-35 minutes after xanomeline or vehicle injection. Signal segments were band-pass filtered (0.5-100 Hz) using a third-order Butterworth filter forward and backward to preserve phase information before down-sampling to a sampling rate of 200 before analyzing the LFP.

Power spectral density

For power spectral density analysis, the 10 s-long, filtered segments of LFP signal were concatenated and the power was calculated for 1 s-long segments using Welch's method with non-overlapping windows. Displayed spectra were multiplied with squared frequency. Example time-frequency plots of power were calculated with a continuous wavelet transformation (Morlet wavelet).

Imaginary coherence

The imaginary part of complex coherence, which is insensitive to volume conduction, was calculated by taking the absolute value of the imaginary component of the normalized cross-spectrum. Group comparisons were carried out on average coherency values of the theta (6-10 Hz), beta (12-30 Hz), and gamma (30-100 Hz) frequency band.

Peak frequency and amplitude

Squared frequency multiplied spectra from either 1–12 Hz or 12–100 Hz were smoothed and peaks with a minimum width of 5 Hz were detected. The most prominent peak in the spectra was defined by the product of peak amplitude, peak half width, and peak prominence (i.e., how much the peak stands out due to its intrinsic height and its location relative to other peaks). The peak frequency corresponded to the resulting x-axis value and the peak amplitude to the average value of the y-axis between +/- 1 Hz of the peak frequency. Peak detection was carried out on the power spectrum of each recording with similar parameters across recordings.

1/f slope

The 1/f slope (power-law decay exponent) of the LFP power spectrum was computed as in Gao et al.[102] A robust linear regression on the log-log transformed power spectrum in the 30 to 50 Hz frequency range was used to determine the slope (see Figure S2E).

Spectral density ratio

SDR was calculated according to a previously published algorithm.[103] To assess the direction of causation we quantified a modulation index between the values for each direction ((area A - area B)/ (area A + area B)) where values above 0 indicate the presence of a directionality from A to B and values below 0 the presence of a directionality from B to A.

Phase-amplitude coupling

PAC was calculated on filtered 10 s-long signal segments using the PAC toolbox based on the normalized modulation index measure as previously reported.[172] Range of phase vector was set to 1 to 12 Hz, and range of amplitude vector was set to 20–100 Hz. Significant coupling was calculated in comparison to a shuffled dataset. Non-significant values were rejected. Group comparisons were carried out on average PAC values between the theta (6-10 Hz) phase and gamma (30-100 Hz) amplitude.

Ripple analysis

Ripple analysis. Ripples were detected using the normalized squared signal by thresholding the baseline, merging neighboring events, thresholding the peaks, and discarding events with excessive duration according to the open access MATLAB code of the Buzsaki lab (https://github.com/buzsakilab/buzcode/blob/master/detectors/detectEvents, function: bz_FindRipples). Thresholds for ripple beginning, end, and peak were set to 2 and 5. Thresholds were computed as multiples of the standard deviation of the normalized squared signal. The minimum ripple interval was set to 100 ms and maximum ripple duration was set to 300 ms.

Single-unit analysis

Spikes were detected with klusta ([173] https://github.com/kwikteam /klusta). Automatically-obtained clusters were then manually curated using phy (https://github.com/cortex-lab/phy). Data were imported and analyzed using custom-written routines in MATLAB. The Fano Factor was quantified as the variability of inter-spike intervals divided by average inter-spike intervals. Only intervals smaller than 1 s were considered.

Spike-LFP coupling

Phase locking of spikes to network oscillations for each channel was assessed by quantifying the mean vector length using the *circ_r* MATLAB function. Briefly, the LFP was filtered for theta (6–10 Hz) and gamma (30–100 Hz) using a third-order Butterworth filter. The instantaneous phase was extracted using the Hilbert transform on the filtered signal. The coupling between spikes and network oscillations was tested for significance using the circ_otest MATLAB function. Phase locking values for all units and percentage of significantly locked units/recording were used to compute group differences.

Statistical analyses of electrophysiological and behavioral data

Statistical analyses of electrophysiological data were performed in MATLAB and R. To test for a significant modulation (*p<0.05, **p<0.01, ***p<0.001) of the SDR data, each group was tested for the hypothesis that their median is zero at the 5% significance level using the Wilcoxon signed rank test (*signrank*) in MATLAB. Statistical differences (*p<0.05, **p<0.01, ***p<0.001) between groups on nested data were analyzed with linear mixed-effect models. Parameter estimation was done using the *lmer* function implemented in the *lme4* R package. To test the significance of condition (group) in the model, a likelihood ratio test against a reduced model was performed in which condition was removed (*lmerTest* R package). For head-fixed data the full model included following parameters: Measured parameters ~ condition + (1 | sex) + (1 | animal) + (1 | recording number). For freely moving data, data were acquired from both brain hemispheres. Therefore, the full model included slightly different parameters: Measured parameters ~ condition + (1 | animal) + (1 | recording number) + (1 | brain area). For multiple group comparisons of xanomeline treated mice, post hoc analysis with Tukey's multiple comparison correction was carried out using the *glht* function of the *multcomp* R package (see Statistics Table S2 for detailed statistics). No statistical measures were used to estimate sample size since effect size was unknown.

Behavioral tests

Pre-pulse inhibition

The pre-pulse inhibition (PPI) test was performed in a MedAssociates ENV-022S Acoustic Startle Reflex box. A background noise level of 62 dB was presented to the mice during a 5-minute acclimation period. All PPI test sessions comprised both startle trials (pulse) and pre-pulse trials (pre-pulse followed by pulse). For pulse trials, a 20 ms pulse at 110 dB was delivered to the animal. During the pre-pulse trials, a 4 ms pre-pulse sound was initially introduced to the animal at intensities of 66, 70, 74, 78, and 82 dB (equating to 4, 8, 12, 16, and 20 dB above the background level, respectively). Subsequently, following a 100 ms interval, a 20 ms pulse at 110 dB was presented. Variations in the delay between each trial were introduced to prevent predictability. Each trial was repeated 10 times. The entire testing procedure required approximately 30 minutes for completion. The calculation of PPI was executed utilizing the following formula:

$$PPI = 100 - \left(\frac{peak\ startle\ response\ prepulse\ and\ pulse}{peak\ startle\ response\ pulse\ alone}\right) \times 100$$

Significant differences (*p<0.05, **p<0.01 and ***p<0.001) between the groups were calculated using aligned rank transform with the *artlm* function of the *ARTool* package. For the peak startle, the significant differences between the groups were calculated using the non-parametric Wilcoxon rank sum test for unpaired data. For the xanomeline experiment, for both the PPI and the peak startle, significant differences were calculated using Kruskal-Wallis rank sum test and Dunn post-hoc tests with Holm correction with the *FSA* package in R Studio.

Latent inhibition

Latent inhibition experiments were conducted within a Campden Instruments Model 80614A TouchScreen apparatus. Foot shocks were administered using a Lafayette Instrument Scrambled Animal Shocker HSCK100AP. The mice were assigned to either a Pre-Exposure (PE) group or a Non-Pre-Exposure (NPE) group. Over the initial three days, following a 5-minute acclimation period, animals in the PE group were exposed to 10-second tones separated by an interstimulus interval (ISI) of 30 seconds. Conversely, the NPE group remained in the apparatus for an equivalent duration without exposure to tones. Concluding the session on the third day, all animals received two 1-second foot shocks, each set at 0.6 mA, synchronized with the tone presentation. On the fourth day, the animals were placed in a distinct context – a black rectangular polyvinyl plastic box. After a 2-minute acclimation period, the animals were subjected to a 3-minute tone exposure, with the event being video-recorded. Subsequently, the video recordings were analyzed utilizing the ANY-Maze software. For analysis, only freezing episodes lasting longer than 1 second were considered. Significant differences (*p<0.05, **p<0.01 and ***p<0.001) between the groups were calculated using non-parametric Wilcoxon rank sum test for unpaired data and the aligned rank transformation with the *art* function of the *ARTool* package and post-hoc tests were performed using the *contrasts* function of the *emmeans* package.

Open field behavior

Open field behavior for head-fixed mice was quantified during recordings within the Mobile HomeCage (Neurotar, Helsinki, Finland). The speed and location of the mice within the 30 cm-diameter arena was monitored with the magnetic tracking capability of the Mobile HomeCage and TTL-synchronized to the recording signal of the Neuralynx amplifier. Significant differences (*p<0.05, **p<0.01 and ***p<0.001) between the groups were calculated using non-parametric Wilcoxon rank sum test for unpaired data.

Locomotor activity, Novel Location Recognition and Novel Object Recognition

The experimental apparatus was a grey polyvinyl plastic square open field (40 x 40 x 40 cm). Habituation training consisted of exposing the mice to the apparatus for 10 minutes, 24h prior to the test. A "center" zone was defined as the area 10 cm away from the walls of the apparatus. Locomotor activity was video-recorded for 10 minutes.

All following trials lasted 10 minutes. During the first day of object testing, animals were placed in the box in presence of two identical objects and allowed to explore them. On the second day of object testing, the position of one of the objects was changed. On the final day of testing, the object in the newer position was exchanged with a differently shaped object. The two identical objects were two rectangular plastic blocks and the third object was a plastic cone of roughly the same height. The exploration time of each object (T) was measured. The discrimination index (DI) was calculated with the following formula:

$$DI = \frac{(T_{novel} - T_{familiar})}{(T_{novel} + T_{familiar})}$$

Videos were analyzed using the ANY-Maze software. Significant differences (*p<0.05, **p<0.01 and ***p<0.001) between the groups were calculated using non-parametric Wilcoxon rank sum test or the Kruskal-Wallis rank sum test and Dunn post-hoc tests with Holm correction with the *FSA* package in R Studio.

Four-choice discrimination and reversal task

The four-choice odor discrimination and reversal task was conducted in P32-33 GFP-calneuron-1 and GFP-control mice as previously described.[174] During the habituation session, four petri dishes (6 cm in diameter) with wooden shavings and a piece of cereal reward (Cocoa Krispies) were placed in a quadratic maze (30 x 30 cm) with 4 separate compartments. During pre-training, one dish with increasing amounts of shavings covering the cereal reward was put in alternating quadrants. For testing the four-choice odor discrimination and reversal, the wooden shavings were scented by mixing them with dried spices (FUCHS Gewürze GmbH) (garlic powder, black pepper, rosemary, thyme - 0.1% by volume and clove - 0.05% by volume). During the initial phase of the test, the animal had to discriminate among four odors and to associate an odor with the buried cereal reward. Each trial was terminated as soon as the mouse made the choice by digging with front paws or nose into the dish and, in case of a correct choice, the food reward was eaten. Once the criterion of 8 out of 10 consecutive correct trials was fulfilled during the discrimination phase, the mouse was immediately moved to the reversal phase. During the reversal phase, one previously unrewarded odor became the rewarded odor, and the other one was exchanged for a novel odor as distraction. To complete the reversal, the mouse had to reach criterion by completing 8 out of 10 consecutive trials correctly. Twenty-four hours before testing, mice were food deprived. Significant differences (*p<0.05, **p<0.01 and ***p<0.001) between the groups were calculated using the non-parametric Wilcoxon rank sum test for unpaired data.

Two choice attentional set-shift task

The two-choice attentional set-shift task[126,127] was conducted in P70-75 GFP-calneuron-1 and GFP-control mice. During the habituation session, two petri dishes (6 cm in diameter) with cat litter or plant granulate as bedding and a piece of cereal reward (Cocoa Krispies) were placed in a rectangular maze (30x40 cm) with 2 separate compartments. During pre-training, two dishes with increasing amounts of both types of bedding covering the cereal reward were put in alternating corners. For testing, the beddings were scented by mixing them with dried spices (FUCHS Gewürze GmbH) (coriander, cumin - 0.1% by volume). During the initial phase of the test, the animal had to discriminate among two odors and to associate an odor with the buried cereal reward. Each trial was terminated as soon as the mouse made the choice by digging with front paws or nose into the dish and, in case of a correct choice, the food reward was eaten. Once the criterion of 8 out of 10 consecutive correct trials was fulfilled during the discrimination phase, the mouse was immediately moved to the set-shift phase. During the set-shift phase, the relevant dimension changed and the

mice had to associate the reward with the type of bedding. To complete the set-shift phase, the mouse had to reach criterion by completing 8 out of 10 consecutive trials correctly. Twenty-four hours before testing, mice were food deprived. Significant differences (*p<0.05, **p<0.01 and ***p<0.001) between the groups were calculated using the non-parametric Wilcoxon rank sum test for unpaired data.

Spatial working memory

At P73-75, mice were positioned in the center of an elevated eight-arm radial maze. Four arms contained a piece of cereal reward (Cocoa Krispies) at the distal end (baited arms). On the first day, mice were allowed to examine the maze for 20 min or until all arms were visited. During the following 10 trials (2-4 trials daily), mice were allowed to examine the maze until all baited arms were visited while arm entries were monitored. The cut-off for terminating a trial before all baited arms were visited was set to a maximum of 20 min or a maximum of 30 entries. Visit of a non-baited arm was considered as reference memory error, repeated visit of the same arm in one trial as working memory error. Throughout behavioral testing, mice had restricted access to food. The amount of food was set to preclude weight loss. Animals were tracked offline using the Python-based tracking system ezTrack ([156] https://github.com/denisecailab/ezTrack). Significant differences (*p<0.05, **p<0.01 and ***p<0.001) between the groups on separate days were calculated using the non-parametric Wilcoxon rank sum test for unpaired data. To test for the condition (calneuron/control)*time effect, the Kruskal-Wallis test with Bonferroni corrected post hoc was used.